Preparation of Functionalized Graphene Sheets

Zdenko Špitalský*, Martin Danko, and Jaroslav Mosnáček

Polymer Institute, Slovak Academy of Sciences, Dubravska cesta 9, 845 41 Bratislava, Slovakia

Polymer Institute, Center of Excellence GLYCOMED, Slovak Academy of Sciences, Dubravska cesta 9, 845 41 Bratislava, Slovakia

Abstract: Graphene is a new and hot research topic due to properties previously not observed on the nanoscale. These properties make graphene a promising candidate for new devices. However, graphene is not soluble, and this property limits its processability. Therefore, chemical functionalization is needed. This short review summarizes the covalent chemical reactions that have been performed on individual graphene sheets – the production of graphene oxide with subsequent transformation to graphene, the covalent modification of graphene oxide functional groups and the surface chemistry of the aromatic rings of graphene sheets.

Keywords: Graphene, graphite, graphene oxide, oxidation, reduction, modification, surface chemistry.

1. INTRODUCTION

Carbon forms many allotropes; three-dimensional allotrope diamond and graphite are known from ancient times, while zero-dimensional fullerenes and one-dimensional nanotubes were discovered in the last century [1-3]. The two-dimensional allotrope-graphene-was first obtained very recently, immediately attracting attention [4]. The number of publications about graphene increased by a factor of 10 in the five years since its discovery according to the Chemical Abstract Service databases [5,6]. The total number of citations per year also dramatically increased as an indication of the increasing scientific impact of graphene research. Now, graphene has become a hot research topic with a strong vow to address the global demand for new and revolutionary materials.

Graphene, consisting of single planar layers of hexagonally arranged sp^2 carbons (it can be viewed as an individual atomic plane extracted from graphite, as an unrolled single-wall carbon nanotube or as a giant flat fullerene molecule), is currently the most exciting carbon-based structure. The coupling of layers is possible due to the weak Van der Waals forces between them. Structures with up to 10 graphene layers are known as few-layer graphenes, while structures with more than 10 and less than 100 layers are considered as thin films of graphite. The number of layers is very important and needs to be controlled because it may determine the properties and performance of the graphitic material. Single graphene was obtained the first time by Novoselov from three-dimensional graphite using a technique called micro-mechanical cleavage [7]. Graphene exhibits a number of exotic physical properties, previously not observed at the nanoscale. The observation of its great mechanical strength of 130 GPa, high Young's modulus of 1 TPa [8], high adsorption of hydrogen and CO_2 [9], room-temperature quantum Hall effect, ultrahigh electron mobility and ballistic transport, long electron mean free paths, zero electronic band gap, superior thermal conductivity and remarkable flexibility are among the striking properties of graphene [5,10].

The unusual electronic properties of this new material make it a promising candidate for future devices. While these applications are a focus of further investigations, there are some areas where graphene can be used directly. Graphene has attracted increasing attention for optoelectronic devices [11], super-capacitors [12,13], gas sensors [14-18], pH sensors [19], chemical sensors [20-23], strain sensors [24], biosensors [25], transparent films for liquid crystal devices [26], biodevices, DNA transistors [27] and nanocomposite applications [28-31]. The proposed applications have enhanced properties comparing to carbon nanotube materials.

The aforementioned method of mechanical exfoliation of graphite (also known as the "Scotch tape" or peel-off method) provided a small amount of high quality samples for fundamental studies. Several other methods were subsequently developed and have been utilized to produce graphene sheets. Reported methods include the chemical reduction of liquid suspension graphene oxide (GO) [32], liquid-phase exfoliation of graphite [33], conversion of nanodiamond [34], epitaxial growth by thermal desorption of Si atoms from the SiC surface, epitaxial growth by chemical vapor deposition on transition metals, solvothermal synthesis and unzipping carbon nanotubes. A discussion about the production of graphene using colloidal suspensions is provided by Park [35].

Despite the number of methods for its synthesis, as-prepared graphene itself is not soluble and thus cannot be dispersed in water or any organic solvent. Suitably modified graphene nanosheets could display good solution chemistry with properties such as dispersability and solubility in water and organic solvents. Therefore, hydrophilic and organophilic affinities for graphene nanosheets should be achievable through chemical functionalization. Despite the recent progress in the production of graphene, the synthesis of uniform and large enough quantities of single-layer graphene is still an ongoing challenge [5]. Many researchers are now focusing on derivatives of graphite, which is inexpensive and available in large quantities. A particularly popular derivative is GO, which is hydrophilic and has a larger interlayer distance than graphite. It can readily exfoliate into individual GO sheets in water and forms stable dispersions after ultrasonication. Subsequent deoxygenation via reduction can restore the electrically insulating GO to conductive graphene [36]. Maintaining the individual separation of the graphene sheets is the most important and challenging aspect of all these synthetic routes. Bulk graphene sheets – if left unprotected – will spontaneously agglomerate and even restack to form graphite. Moreover, neat graphene is an insoluble and relatively inert material. Chemical functionalization or the use of dispersant is generally needed to prevent agglomeration [31,37,38]. The GO synthetic pathway is attractive for stabilizing individual sheets in solutions. The oxygen functional groups that exist in GO provide reactive sites for chemical modification using known carbon surface chemistry. The chemical attachment of appropriate organic groups leads

*Address correspondence to this author at the Polymer Institute, Slovak Academy of Sciences, Bratislava, Slovakia; Tel: +421-2-5477 3308; Fax+421-2-5477 5923;
E-mail: zdeno.spitalsky@savba.sk

1385-2728/11 $58.00+.00

Table 1. The Analysis of Dried GO Prepared by Different Methods According to [51,53,54]

Method	C [wt %]	O [wt %]	H [wt %]	Water [wt %]	Ash [wt %]	C/O Atomic Ratio
Preoxidation of Hummers - Offeman	45.2	46.5	2.3	-	-	1.3
Hummers - Offeman	47.06	27.97	-	22.99	1.98	2.25
Staudenmaier	52.11	23.99	-	22.22	1.90	2.89
Brodie	60.74	37.41	1.85	-	-	-

to physical separation of the resultant graphene sheets but also makes it possible to directly form stable graphene dispersions during the synthetic process. The successful dispersion of graphene has enabled the use of low cost solution processing techniques to fabricate various potentially useful graphene-based materials [36].

Although there are some reviews describing the intercalation of graphite or exfoliated graphite (exfoliated graphite is a highly porous, low dense material consisting of several-nanometer-thick multilayer stacks that is prepared by the thermal decomposition of graphite intercalation compounds) [39-43] or chemical modifications of graphitic surfaces, such as carbon nanotubes [44,45], glassy carbon, highly ordered pyrolytic graphite, carbon black or pyrolyzed photoresist films [46], a comprehensive overview about neat graphene is missing. Based on the structural similarity of the aforementioned graphitic structures it is possible to predict that the organic chemistry of individual graphene sheets or graphene nanoplatelets will also be similar. Therefore, here we give an overview of the different synthetic strategies leading to functionalized individual graphene sheets. This short review tries to summarize only reactions performed on individual graphene sheets or on carbon materials that, under the reaction conditions, are transformed into modified individual graphene sheets. The review is divided into three parts: the preparation and properties of GO, its reduction to neat graphene and other covalent modifications of graphene nanoparticles. Detailed descriptions of the modifications and reaction products are given. The last part is divided into two categories: reactions of the functional groups of GO and reactions of the aromatic rings of graphenes.

2. CHEMICAL MODIFICATION

2.1. Oxidation – Preparation of Graphene Oxide (GO) and its Properties

The GO formation involves the reaction of graphite with strong oxidizers. The introduction of oxygen containing functional groups, such as hydroxyl and epoxide, results in an increase in the interplanar/interlayer spacing of GO as well as a change of hybridization of the oxidized carbon from planar sp^2 to tetrahedral sp^3. In analogy to carbon nanotubes [47,48], GO can assemble into paper-like materials under a directional flow and has very high values of tensile modulus and fracture strength [49,50].

GO (sometimes called graphite oxide, graphitic oxide or graphitic acid) has been known for more than one and a half centuries. It was first prepared by Brodie [51] in 1859 by repeated treatment of graphite with an oxidation mixture of potassium chlorate and fuming nitric acid. The methods most commonly used at present time are the original Brodie synthesis, one described by Staudenmaier [52] in which the graphite is oxidized in concentrated sulfuric and nitric acids with potassium chlorate, and one described by Hummers and Offeman [53] in which the graphite is treated in a water-free mixture of concentrated sulfuric acid, sodium nitrate and potassium permanganate, respectively. Later it was found that an additional graphite oxidation with persulfate was needed prior to the GO preparation of Hummers and Offeman. Without this additional oxidation, incompletely oxidized graphite-core/GO-shell particles were always observed in the final product [54]. Recently the Hummers-Offeman method was modified by microwave heating [55]. With this newest approach it is possible to produce gram quantities of large, single layer GO membranes, up to 2000 μm^2 in size, in a yield exceeding 90%. The microwave pre-exfoliation of graphites enabled a faster and more uniform functionalization under milder conditions.

The first two methods (Brodie and Staudenmaier) are considered as hazardous and have to be performed with constant cooling. The processes are time consuming and explosive chlorine dioxide is evolved. The processes also require more than 10 grams of potassium chlorate for each gram of treated graphite. The Hummers-Offeman procedure requires less than two hours for complete conversion at temperatures below 45°C and can be carried out safely. Well reacted samples of GO will have a carbon to oxygen atomic ratio between 2.1 and 2.9. The color of the product when suspended in water may be used as a criterion for the degree of oxidation of the graphite. The product richest in GO will have a bright yellow color whereas poorer samples with higher carbon/oxygen ratios will have a green to black hue. An analysis of the dried GO prepared by the above mentioned methods is compared in Table (**1**). Brodie`s GO is insoluble in water containing acids or salts but is very slightly soluble in pure water. The crystals placed on litmus paper undergo a feeble acid reaction. It combines with alkalis. When agitated with dilute ammonia it is converted into a transparent jelly, but it does not dissolve [51]. It is very hygroscopic [56] and can accommodate up to 12 wt% water within its structure [57]. Studies on the surface charge (zeta potential) of as-prepared GO sheets showed that these sheets are highly negatively charged when dispersed in water, an apparent result of the ionization of the carboxylic acid and phenolic hydroxyl groups. This result suggests that the formation of stable GO colloids could be attributed to electrostatic repulsion rather than just the hydrophilicity of GO [58].

A three stage mechanism was suggested by Rodríguez and Jiménez to explain the oxidation of graphite in liquid media [59]:

1) An initial period - functional groups are simply attached to the layer edges. The samples have hardly obtained any oxidizing capacity.

2) An intermediate period - oxidizing capacities increase to the values characteristic for GO.

3) A final period that includes the most strongly oxidized samples. The oxygen and hydrogen contents have reached their maximum values in the characteristic range for GO. However, some groups within the layers still undergo chemical transformations. Carboxyl groups (-COOH) appear in this last stage of oxidation attack when layers are cleaved and separated to a distance characteristic for GO.

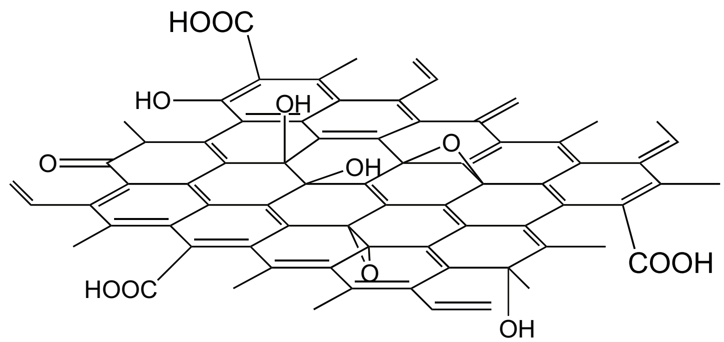

Fig. (1).

Prolonged oxidation affords higher acidic strengths to the GOs, resulting in a nearly linear decrease in pH [60]. It was found during optical microscopy observations of the oxidation stage of the Hummer–Offeman method that the invasion speed of the oxidant into the natural graphite particles was about 10 $\mu m.h^{-1}$ or more [61].

A slower oxidation rate for natural graphite relative to synthetic graphite was observed. The slower rate was explained by the larger layers and their more perfect arrangement in natural graphite [59,62]. It was observed that there is no significant size difference in the GO products as the size of the starting graphite flakes is changed, suggesting that the product size is intrinsically determined by the oxidation process [63]. During the first stage of thermal decomposition an endothermic effect due to dehydration occurs. In the second stage (200-240°C) the thermal decomposition of GO occurs. In this case CO_2 and CO, in addition to water, evolve. This stage (internal combustion or proper decomposition) is not finished at 270°C, when a portion of the decomposition product was taken. The third stage is combustion and does not occur under an inert atmosphere. The combustion of the carbonaceous residue in the air begins at variable temperatures (ranging from 540 to 700°C) that are higher in the most oxidized compounds and indicate tautness in the layers of the intermediate oxidation products. In the air, the ashes at 800°C are always smaller than 1% of the initial weight [59,62]. The results from thermal analyses agree with this mechanism. Only the strongly oxidized samples deflagrate upon rapid heating. There is a temperature of flash decomposition when deflagration occurs. This temperature has been used in the characterization of GOs and corresponds to 170°C for GO obtained by the Hummers-Offeman method, 210°C for GO obtained in anhydrous nitric acid and 230°C for GO obtained by the Staudenmaier method [62].

The Klinowski group studied GO and its derivatives using ^{13}C and ^{1}H NMR [56,64]. They found that the concentration of isolated C=C double bonds is likely to be very low, as they are easily oxidized, and varies with the degree of GO oxidation. The formation of phenol (or aromatic diol) groups during deoxygenation indicates that the epoxide and the C-OH groups are very close to one another. Apart from the double bonds, the "oxidized" benzene rings contain epoxide (1,2-ethers and not 1,3-ethers) and C-OH groups. It is not necessary for the distribution of functional groups in every oxidized aromatic ring to be identical, and both the oxidized rings and aromatic entities are distributed randomly. The layers of GO are terminated with C-OH and -COOH groups, consistent with infrared (IR) spectroscopic results. The structure of GO contains two kinds of regions: aromatic regions with unoxidized benzene rings and regions containing aliphatic six-membered rings. The relative sizes of the two regions depend on the degrees of oxidation. Aromatic entities, double bonds and epoxide groups give rise to a nearly flat carbon grid. Only the carbons attached to OH groups are in a slightly distorted tetrahedral configuration, resulting in some wrinkling of the layers. The functional groups lie above and below the carbon grid and form a layer of oxygen atoms of variable concentration. This arrangement of negatively charged oxygen layers could prevent the nucleophilic attack on carbon atoms and explain the relative chemical inactivity of the epoxide groups of GO. This structural model of GO is often called the Lerf-Klinowski model (Fig. **(1)**). Additional analysis confirmed these assignments [65]. Although this model is one of the most used in the literature, there are some other models [66,67].

The Fendler group studied preparation of ultrathin films layer-by layer self-assembled from GO and poly(ethylene oxide) or poly(diallyldimethylammonium chloride) [68,69]. Part of this research was the study of graphite oxidation to different extents by the Brodie method. The authors observed [68] that the interlayer spacing of the untreated graphite (initially close to 3.34Å) expanded upon oxidation up to 3.49Å depending on the degree of oxidation. These data indicated that the oxidative treatment had an important effect on the thickness of the nanoplatelets, diminishing it with the extent of the oxidation. The p*K*a values ranged between 6 and 7. Unexpectedly, the number of exchangeable protons and the charge density decreased with the extent of oxidation relative to the hydrogen content of the GO powders, indicating that the carboxyl groups became more labile upon further oxidation. However, the atomic ratio of [O]/[C] increased linearly with the number of oxidative steps.

Fiang with Beck prepared GO with the nominal composition C_8OH and $C_{2.65}OH$ by anodic oxidation of natural graphite in 96% H_2SO_4 [70]. The degree of oxidation was controlled potentiostatically or galvanostatically. Their results support the conclusion that the formation of GO goes through the graphite intercalation compound intermediate. The electrochemical oxidization of graphite in an ammonia medium was successful for the exfoliation of graphite, producing exfoliated nanoparticles of about 40 nm in diameter [71]. Those nanoparticles consisted of single layer as well as multilayer sheets that contain oxygen-containing functional groups derived from the oxidization of graphite. The presence of polar groups made the nanoparticles dispersible in water, leading to colloid formation of the exfoliated graphite derivatives.

2.2. Transformation of GO to Graphene

The reduction of GO leads to graphene or materials that on the microscopic level is structurally similar to neat graphene. Different reagents can be used and the final chemical structure of the graphene is dependent on the type of reagent. The reactions can be performed on GO nanoparticles dispersed in media, but the resulting graphene re-agglomerates. When GO is embedded in a solid matrix, the reaction leads to individually dispersed graphene nanoparticles that are unable to agglomerate.

Reagents that can be used include ammonia (gas or solution) and chlorine (gas). Elemental analysis confirmed that the product after treatment with ammonia did not contain a lower proportion of oxygen. A lower epoxy content and greater hydroxyl content was found for all of these compounds. The action of chlorine on GO did not seem to modify any physical characteristics of the compound. Nevertheless, there was an increase in epoxy group content and a decrease in C-OH and C=C group content [57].

GO was pyrolyzed by heating it under a dynamic vacuum at 300°C for 10 hours [72]. The composition of the resulting sample was $C_{21}O$, indicating that it contained no hydrogen and very little oxygen. The number of lost carbon atoms was determined to be one fifth of the number of total carbon atoms. Rapid heating (>2000°C.min^{-1}) to 1050°C and purging with argon split GO into individual sheets with the evolution of CO_2 [73]. Because of the elimination of oxygen from functional groups and any residual water during the rapid heating, elemental analysis showed an increase in the C/O ratio from 2:1 in GO to 10:1 in the reduced state. Similar results were obtained in an argon-hydrogen (8:2) atmosphere at 500 and 1000°C for 5 minutes [74].

One possible reagent for transformation of GO to a graphene-like material is potassium iodide (KI). Elemental analysis showed that the reaction of GO with KI in an acidic medium led to a product that still contained oxygen and hydrogen [59], but the residues had a graphite-like external appearance.

The reduction performed with nascent hydrogen from aluminum powder and hydrochloric acid resulted in a "random-shape-aggregate" [61]. The scanning electron microscopy (SEM) image clearly indicated that singular or plural aggregates of the thin-film particles irregularly bent and deformed. This shows that when the affinity between the particles and the dispersion medium is very low, the reduced graphene particle(s) aggregates like a linear flexible polymer. In addition, X-ray powder diffraction (XRD) profiles revealed a complete disappearance of the peak corresponding to 0.83 nm, which was observed in the original oxidized thin-film particles. This property is the result of the deformation and aggregation of particles that lowered the degree of both interparticular orientation and interlayer orientation inside each particle.

A stable water dispersion of GO nanoplatelets, prepared by exfoliation of the GO (1 mg.ml^{-1}) via sonication, was treated with hydrazine hydrate at 100°C for 24 hours [37]. Dimethylhydrazine can also be used as a substitute for hydrazine (hydrazine is highly toxic and dangerously unstable, especially in the anhydrous form) [29]. As the reduction proceeded, the brown-colored dispersion of exfoliated GO turned black and the resulting nanoplatelets agglomerated and eventually precipitated. This precipitated material could not be re-suspended even after prolonged sonication in water in the presence of surfactants such as sodium dodecylsulfate (SDS) and TRITON X-100, which have been found to successfully solubilize carbon nanotubes. Elemental analysis of both GO and the treated material indicated that there was a considerable increase in the C/O atomic ratio in the reduced material (10.3) compared to that in the starting GO (2.7). Hence, the treated material can be described as consisting of partially oxidized graphitic nanoplatelets, given that a fair amount of oxygen is retained even after the reaction. The black color of the treated materials suggested a partial re-graphitization and reduction of the exfoliated GO. In addition to the decrease in the oxygen level, reduction of GO was accompanied by nitrogen incorporation from the reagent (C/N = 16.1). GO dispersions with concentrations less than 0.5 mg.ml^{-1} can also be treated with hydrazine in alkaline ammonia solution. The particle size of the resulting graphene sheets did not increase after the reduction was complete [58]. No sediment was observed even after the dispersion had been centrifuged at 4 000 rpm for several hours. Atomic force microscopy (AFM) showed that the resulting sheets were flat, with a thickness of ~1 nm. As was the case for the original GO dispersions, these results indicated that thus obtained graphene sheets remained separated in the dispersion without the need for either polymeric or surfactant stabilizers. The treatment with 1 vol% hydrazine solution in dimethylformamide (DMF) at 80°C for 24 hours resulted in a pronounced increase of conductivity [75]. The conductivity of the hydrazine-treated GO monolayers was approximately 3 orders of magnitude higher compared to the starting GO. Room temperature measurements of more than 50 treated GO monolayers yielded conductivity values between 0.05 and 2 S.cm^{-1}. This range is about 3 orders of magnitude below the values reported for pristine graphene. It is worthy to note that even on the same substrate, the conductivity of different monolayers varied by up to 1 order of magnitude. The hydrazine-treated GO samples showed a significant reduction in conductivity by more than 3 orders of magnitude upon cooling from 298 to 4 K. This result is in contrast to the conductivity of unmodified graphene, which was reduced by less than 1 order of magnitude. Despite the different temperature dependencies of electrical conductivity, the reduced GO monolayers showed ambipolar behavior in the gate dependence of resistance that was similar to that of pristine graphene. The reduction of GO by exposure to hydrogen plasma (30W at a pressure of 0.8 mbar) for 5-10 seconds at room temperature was performed alongside this reduction. Similar results were obtained for the treatment of GO with hydrazine hydrate in water [32]. GO was also modified by exposure to hydrazine vapor for 20 hours [76]. Hydrazine vapor was generated by bubbling nitrogen gas through a plastic tube containing liquid hydrazine hydrate. This gas then flowed over the GO sheets, which were heated to 85°C to prevent the hydrazine vapor from condensing. It was found that the hydrazine vapor alone was not sufficient to achieve the high yield reaction, and annealing alone required relatively high temperatures. Efficient transformation of the GO to graphene was therefore achieved through a combination of hydrazine vapor exposure and annealing treatment [77,78]. The result was a graphene with sheet resistivity in the range of 10^2-10^3 Ω.square^{-1} with 80% light transmittance. It was later discovered that the thermal treatment was more effective in restoring electrical conductivity than was the chemical treatment with hydrazine [79].

Attempts to transform GO into graphene in the presence of SDS and TRITON-X100 also failed to produce a stable aqueous dispersion of graphitic nanoplatelets. However, when the treatment was carried out in the presence of amphiphilic polymer - poly(sodium 4-styrenesulfonate) (PSS) - a stable black dispersion was obtained [37]. This dispersion can be filtered through a membrane to yield PSS-coated graphitic nanoplatelets that can be readily re-dispersed in water upon mild sonication, forming black suspensions. At concentrations lower than 0.1 mg.ml^{-1}, the dispersions obtained after a 30-minute ultrasonic treatment appeared to be indefinitely stable - samples prepared over a year ago are still homogeneous to date. More concentrated dispersions developed a small amount of precipitate after several days. However, they never fully settle, even upon months of standing. Elemental analysis of the PSS-coated platelets indicates that they contained ~40% polymer as judged by their sulfur content. The C/O atomic ratio in the product platelets alone is thus 9.3 (C/N ratio = 22.1), suggesting that a significant reduction of exfoliated GO platelets did take place in the presence of the polymer. That a large concentration of PSS is required to prevent the agglomeration of the platelets during reduction while only a fraction of that amount (5.8% by weight of the PSS employed is absorbed on the reduced GO) is needed to render the complex dispersible indicates that the self-association between reduced GO platelets is a more favorable process than their association with PSS. During the reduction, the polymer needs to be present at a sufficient concentration for its interaction with the surfaces of the platelets to effectively compete with the hydrophobic interaction between the platelets. However, once PSS is attached to the platelet surface, further agglomeration of the platelets is stopped. When treatments were carried out without any PSS, the platelet agglomeration was irreversible: sonication of the reduced material after agglomeration in the presence of excess PSS did not result in platelet dispersion to any extent. The AFM image of the exfoliated GO revealed nanoplatelets of uniform thickness (~1 nm). In the case of PSS-coated reduced GO, nanoplatelets with a thickness of ~4 nm were observed [37].

The reduction of GO in the polyelectrolyte/GO films to graphene was accomplished either chemically or electrochemically [80]. The chemical reduction involved the immersion of the self-assembled film into an aqueous hydrazine hydrate (50%w/v) solution for 1-24 hours or into a 0.10 M HCl solution containing Zn powder (i.e., into a nascent hydrogen generator) for 2-3 hours. The electrochemical reduction of GO (in the polyelectrolyte/GO film, self-assembled on metal or glassy carbon electrodes) was performed by scanning the potential from +0.7 V to -1.5 V vs. a standard calomel electrode and was monitored by cyclic voltammetry. The peak at 0.95 ± 0.05 V corresponded to the electrochemical reduction of GO to graphene. The amplitude of the peak was found to increase initially with the number of GO layers; it levels off when the number of layers reaches 8-10 units. Interestingly, the electrochemical reduction of GO is an irreversible process, as indicated by the featureless reverse scan from -1.3 V to +0.7 V**.** Both chemical and electrochemical reduction were accompanied by a drastic darkening of the film. X-ray diffraction measurements indicated that the reduction of GO to graphene was accompanied by a slight decrease in the interlayer spacing (from 45.2 Å to 43.7 Å for the hydrazine reduction, and from 56 Å to 45 Å for the electrochemical reduction). The resistivity value dropped to 12 kΩ after reduction by hydrogen, evolved *in situ*, amounting to a 27 000-fold decrease in the overall resistance. This corresponds to a change in volume conductivity from $1.2 \times 10^4 \Omega^{-1}m^{-1}$ to $3.1 \times 10^7 \Omega^{-1}m^{-1}$. Similar results were also observed for polycation/GO films [54]. Similarly, when polyaniline-intercalated GO was reduced in aqueous hydrazine hydrate (50% w/v) solution for 24 hours the conductivity increased 26-fold from 1.45×10^{-3} S.cm^{-1} to 3.73×10^{-2} S.cm^{-1} at ambient temperature [81].

The chemical reduction of GO to graphite (re-agglomerated graphene) by either sodium borohydride ($NaBH_4$) or hydroquinone was also performed [82]. The $NaBH_4$ treatment eliminated all oxygen-containing groups. While the parent GO contains 61% C, with the remaining 39% being oxygen and hydrogen (prepared by Brodie method), the reduced solid is composed almost entirely of carbon (98.5% C). Thus, the analysis pointed to the chemical reduction of GO to turbostatic (randomly ordered) graphite by $NaBH_4$. In contrast, the treatment of GO with hydroquinone led to a crystalline and not a turbostatic graphite under soft thermal conditions. Although the mechanism of reduction was unclear, the authors believed that the formation of reactive radicals must play a key role in the observed transformations. It is worth noting that the chemical reduction of GO to graphite can also be achieved by employing either metallic iron or zinc fine powder (resulting in turbostatic graphite) or sulfide ions from Na_2S (resulting is turbostatic graphite) as reducing agents. In all instances, the as-made graphene solids were infrared inactive.

The stable graphene suspensions could be quickly prepared by simply heating an exfoliated-GO suspension under strongly alkaline conditions at moderate temperatures (50–90°C) [83]. The addition of NaOH to the GO suspension was accompanied by a fast, unexpected color change (from yellow-brown to homogeneous black). Careful experiments revealed that exfoliated GO can undergo fast disproportionation with deoxygenation in strongly alkaline solutions, resulting in stable aqueous graphene suspensions. After the reaction, the exfoliated GO showed a significant reduction in the amount of epoxide and hydroxyl groups present. In addition, many sp^2 carbon atoms were introduced, suggesting the formation of graphene-based materials. This result was confirmed by X-ray photoelectron spectroscopy (XPS) analysis, which shows that the O/C ratio in the exfoliated GO decreases after the reaction. Remarkably, the π–π^* peak, characteristic of aromatic or conjugated systems, resumes after the reaction. These results, combined with XRD and thermogravimetric analyses (TGA), indicate the formation of graphene. The graphene suspensions obtained showed impressive long-term stability (several days), which is desirable for processing. Considering the incomplete removal of the negatively charged oxide functional groups, this stability can be attributed to a strengthened electrostatic stabilization under alkaline conditions, as the repulsion between negatively charged graphene sheets should increase at higher pH values. The single-sheet nature of the graphene obtained was confirmed by AFM. The thickness of the graphene sheet was about 0.8 nm. Notably, the reaction can even start at temperatures as low as 15°C when the pH of the suspension is high enough.

Rapid and mild thermal transformation of GO to graphene-like material was achieve with the assistance of microwaves in a mixed solution of N,N-dimethylacetamide and water [84]. The mixed solution worked as both a solvent for the graphene produced and a medium to control the temperature of the reactive system up to 165°C. The reduction time was on the scale of minutes. The conductivity of graphene paper prepared by the microwave reduction method was increased by about 10 000 times that of GO paper. The degree of reaction was similar to that of the typical alkaline chemical reduction process [83].

A novel approach was used in preparation of poly(arylene disulfide)/carbon nanosheet composites [85] with GO acting as an oxidizing reagent for the *in situ* polymerization of aromatic dithiols while the resulting reduced GO acted as the host for the composites. Raman spectra of the carbon host suggested that a zigzag array structure of GO changed into a planar graphene sheet structure in the composites. GPC analysis of the prepared nanocomposites showed that the average molecular weight (M_w) of the soluble part of the resulting nanocomposite was 14 501 g.mol^{-1} (M_n = 10 704 g.mol^{-1}), indicating that the *in-situ* redox reaction between the GOs and the aromatic dithiolic salts produced macromolecules of poly(arylene disulfide). A similar approach was used for the production of graphene/SnO_2 nanocomposites, in which GO was reduced by $SnCl_2$ to graphene sheets in the presence of HCl and urea [86]. The reduction process was accompanied by the generation of SnO_2 nanoparticles.

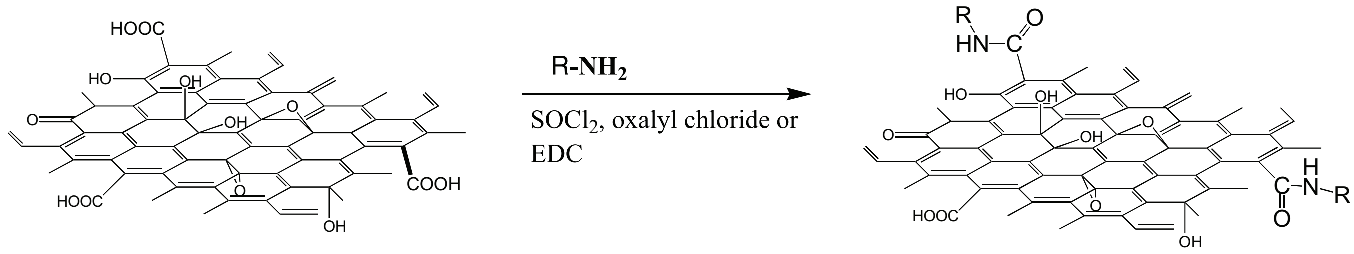

EDC - N-(3-Dimethylaminopropyl)-N'-ethylcarbodiimide hydrochloride

Scheme 1.

The GO in the GO-titanium oxide (TiO_2) nanocomposites was successfully reduced by UV-assisted photocatalytic reduction without the need for hazardous chemicals or high temperature annealing [87]. Charge separation occurred upon UV-irradiation of the TiO_2 particles. In the presence of ethanol, the holes were scavenged to produce ethoxy radicals and electrons accumulated within the TiO_2 particles. These accumulated electrons interacted with GO sheets to reduce certain function groups. The sheet resistance became 45 times lower after 2 hours of UV-irradiation. A reduction process where GO can be photothermally reduced upon exposure to a xenon flash under ambient conditions was performed [88,89]. The direct interaction between TiO_2 particles and graphene sheets hindered the collapse of the exfoliated sheets of graphene. After UV-irradiation the suspension remained stable for about an hour. A slow settling of the composite was seen after this period. Stirring or mild sonication of the TiO_2-graphene sample facilitated re-suspension. Irradiating the suspension for two hours resulted in an order of magnitude decrease in the resistance [89]. Elemental analysis showed that the C/O atomic ratio was increased from 1.15 for GO to 4.23 for flash-reduced GO [88]. Because flash reduction is triggered by light, it has a great advantage over conventional GO reduction processes in that it readily allows photopatterning.

2.3. Covalent Functionalization of Graphene

Graphene sheets of non-oxidized graphene, GO and reduced GO can be further functionalized by chemical reactions with various functional groups. The carboxylic, hydroxyl and epoxy groups present on the basal plane or edges of the graphene sheets of GO allow for functionalization of the graphene by simple organic reactions. Moreover, some organic reactions can also proceed on the aromatic entities of GO or its reduced (non-oxidized) form.

2.3.1. Reactions on Oxidized Carbons of GO

A simple method often used for the functionalization of graphene is based on reactions of the carboxyl groups, present in GO and located at the edges of graphene sheets, with various amines or alcohols. Reactions of the graphene carboxyl groups with amines, leading to the formation of amides, were performed via various more reactive intermediates (see Scheme (**1**)). Subrahmanyam *et al.* reported the functionalization of exfoliated GO and graphene prepared by the thermal conversion of nanodiamond (DG) [9]. Both types of graphene possessed 3 to 6 graphene layers as observed by AFM. To prepare graphene soluble in non-polar solvents, the acid-treated graphene was reacted with an excess of thionyl chloride ($SOCl_2$) and subsequently heated with dodecylamine. It was noted that DG required a harsher acid treatment over longer periods to enable its further functionalization. The functionalization was confirmed by a shift in the C=O stretching band to 1650 cm^{-1} due to the amide band and an appearance of C-H and N-H stretching bands at 2800 and 3300 cm^{-1} as observed by FT-IR spectroscopy. Dodecylamide-functionalized graphenes were readily dispersible in dichlormethane, carbon tetrachloride (CCl_4) and tetrahydrofuran (THF).

A similar approach via an acyl chloride intermediate was also used for the modification of graphite oxide with octadecylamine (ODA) [38,90]. The functionalization was again confirmed by FT-IR spectra measured in a CCl_4 solution at a concentration of 0.156 mg/ml, where the asymmetric C-H stretch of the alkyl groups at 2854 and 2918 cm^{-1} was observed. Moreover, a peak at 1653 cm^{-1} corresponding to the carbonyl stretch of the amide was present in the FT-IR spectra. As reported by Niyogi [38], based on TGA analysis the product showed 7 wt% loss due to the oxidative decomposition of the organic functional groups. AFM images of samples prepared from THF solutions showed the irregular graphite crystallites with thicknesses of 1.5-2.5 nm in addition to single layer graphene sheets. ODA functionalized GO had a solubility of 0.5 $mg.ml^{-1}$ in THF and was also soluble in CCl_4 and 1,2-dichloromethane.

Novel graphene nanohybrid materials with increased non-linear optical performance were prepared using the same approach by activation of carboxyls with $SOCl_2$ and their subsequent reaction with either amino-porphyrine (APP) or pyrrolidine-fullerene [91,92]. In these cases triethylamine was also used as a scavenger of HCl. The presence of a porphyrine ring in graphene/APP adducts led to changes in the absorption band at 268 nm related to graphene, while the APP Soret absorption at 419 nm did not change. On the other hand, the fluorescence of the APP moiety in graphene/APP adducts was quenched and shifted to lower wavelengths. These typical changes are related to photoinduced electron transfer or energy transfer quenching between porphyrine fluorophores and highly π-conjugated carbon-based materials such as graphenes, carbon nanotubes or fullerenes. In FT-IR spectra, new bands at 1640 and 1260 cm^{-1}, corresponding to the C=O and C-N stretching bands of the amide groups, respectively, appeared after functionalization of graphene with amino-porphyrine. Similarly, for pyrrolidine-fullerene-functionalized graphene a broad peak at 1725 cm^{-1}, which was attributed to the overlapping of the remaining carboxyl group in the graphene with the ester group present in the pyrrolidine-C_{60} group, was observed in the FT-IR spectra along with a new peak at 1636 cm^{-1} from the newly formed amide carbonyl group. On the basis of UV spectra and elemental analysis of carefully purified products, one fullerene unit per 104 carbon atoms and one porphyrin unit per 874 carbon atoms of the functionalized

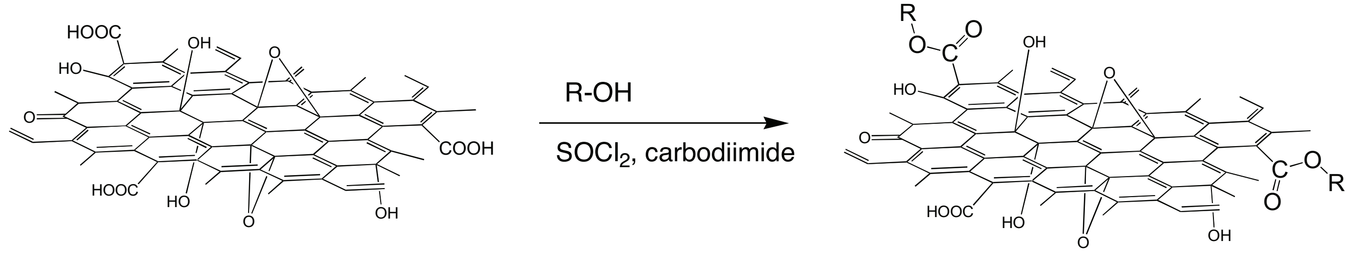

Scheme 2.

graphene were estimated. Both types of functionalized graphene were soluble in DMF and other polar solvents.

Oxalyl chloride was also used for the activation of carboxyls on exfoliated GOs prior to condensation with the $–NH_2$ group of 1-(3-aminopropyl)imidazole [93]. Subsequent N-alkylation of the imidazole ring allowed for the preparation of hybrid graphene materials with an ionic liquid functionality of the imidazolium/counter anion moiety. These materials had advantages that include the modulation of wettability and introduction of extra functionality. The successful formation of ionic liquid graphene hybrid materials was confirmed by ATR-IR and Raman spectroscopy. In the ATR-IR spectra the characteristic carbonyl moiety from the amide bonds appeared at 1640 cm^{-1}. In addition, the C-H stretching vibrations from alkyl chains of alkylated imidazole groups in the 2900-2980 cm^{-1} region were detected. In Raman spectra a broadening of the G-band and their shift to a higher frequency of 1595 cm^{-1}, a growing intensity of the D-band and a broadening and blue shifting of the 2D-band were observed after functionalization of the graphite. Excitation of the porphyrin counter anion in imidazolium-modified GO at 408 nm gave an emission at 630 nm, even though the originally strong emission of the free disodium porphyrin was significantly depressed and broader in the hybrid material due to quenching by graphene. The prepared hybrid material formed stable dispersions in DMF and water (0.8 $mg.ml^{-1}$) and exhibited 9 % loss of organic moieties by TGA analysis. AFM images were representative of single and/or bilayers of exfoliated, modified graphene sheets.

Liu *et al.* used a carbodiimide-catalyzed amidation of single-layered and few-layered GOs to modify the GO with six-arm poly(ethylene glycol)-amine terminated stars [94]. PEGylation was confirmed by ATR-IR spectroscopy of water solutions (3 $mg.ml^{-1}$), where the peaks at 2850 and 1100 cm^{-1} from C-H and C-O bonds of PEG were observed in PEGylated GO. The particle size of the modified GO, as estimated from the AFM images, was 5-50 nm. While non-functionalized GO aggregated in solutions rich in salts and proteins, such as cell medium or serum, due to the screening effect of the electrostatic charges and nonspecific binding of proteins to the GO, PEG-functionalized GO exhibited excellent stability in all biological solutions including serum. The modified GO was subsequently used in a conjugation reaction with a hydrophobic (aromatic-based) drug, SN38. While the enhanced water solubility of GO-PEG was not discussed there, the solubility of the SN38/GO-PEG complex was ~ 1 $mg.ml^{-1}$ (in terms of SN38), which is several times higher than the solubility of free SN38.

The reaction of the graphene carboxyl groups with poly(vinyl alcohol) (PVA; M_w ~ 89 - 98 kDa) was performed using either a direct esterification or through preparation of the acyl chloride and subsequent esterification (see Scheme (**2**)) [95]. Similarly to PVA, the final modified GO was soluble in DMSO and water with the aid of heat. From the ^{1}H NMR spectra, where a decrease in the ratio of *iso* to *syndio* triad signals was observed after functionalization, it was concluded that the esterification reaction occurs in the isotactic configuration of PVA. Based on the new signal at 4.2 ppm (very close to the *rr* triads) related to the hydroxyl protons next to the acetate groups, a PVA functionalization of around 1.8% was calculated. The authors demonstrated that the degree of functionalization depends on the tacticity of PVA even though the number of carboxylic groups in GO is quite high. FT-IR spectra showed the formation of the C=O stretching band of the ester group at 1715 cm^{-1} as a confirmation of covalent bonding. Moreover, the decrease in the intensity ratio of C-O bands of doubly H-bonded OH in crystalline regions (1144 cm^{-1}) and unbonded hydroxyl groups in amorphous zones (1096 cm^{-1}) after esterification suggested a large decrease in the degree of crystallinity of the modified PVA. Finally, it was reported that its solubility in water was also retained after reduction of modified GO with hydrazine.

The covalent bonding of PVA (M_w ~ 70 - 90 kDa) onto graphene sheets through an esterification process was also reported by Veca *et al.* [96]. They effected the covalent functionalization through a carbodiimide-activated esterification reaction. The presence of ester linkages was confirmed by FT-IR spectra, where a peak at 1730 cm^{-1} characteristic of the C=O stretching mode was observed. ^{1}H NMR spectra showed the diminishing peaks of all three hydroxyl protons in functionalized PVA at 4.2 ppm, 4.5 ppm and 4.7 ppm, related to the isotactic, heterotactic and syndiotactic triads, respectively. According to TGA the functionalized sample contained about 15 wt% carbon nanosheets, almost one order more than that reported by Salavagione [95]. The PVA-functionalized nanosheets were readily dispersed in DMSO or hot water to form stable solution-like dispersions. The thickness of the functionalized nanosheets was measured by transmission electron microscopy (TEM) imaging on the order of 5 nm, which corresponds to around 6-7 graphene layers.

The poly(ethyleneglycol) (PEG) functionalization of graphene was also done *via* the esterification of carboxyls with the hydroxyl end-groups of PEG [9]. The authors used this modification to increase the water solubility of graphene prepared by the acid-treatment method. The height of the graphite particles was 4-5 nm, corresponding to 3-6 graphene layers. Reactions were performed with an excess of PEG at elevated temperature (100 °C) in the presence of HCl. The structural characterization of the PEGylated graphene was not provided.

Some reagents, such as isocyanates, can react with both the edge carboxyl and surface hydroxyl groups of GO (see Scheme (**3**)). The ability of isocyanates to react with hydroxyl groups, which unlike carboxyl groups are also located on the basal plane of the graphene sheets, allows for a higher degree of GO functionalization and thus also better dispersability of large graphene sheets. The chemical modification of GO by aryl and alkyl isocyanates led to the hydrophobization of GO that was readily dispersible in water before the modification [97,98]. The structural changes that oc-

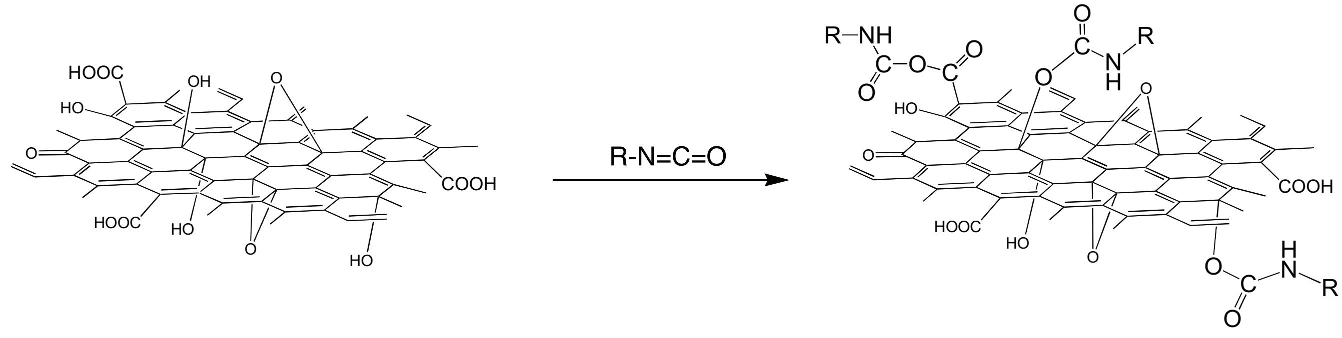

Scheme 3.

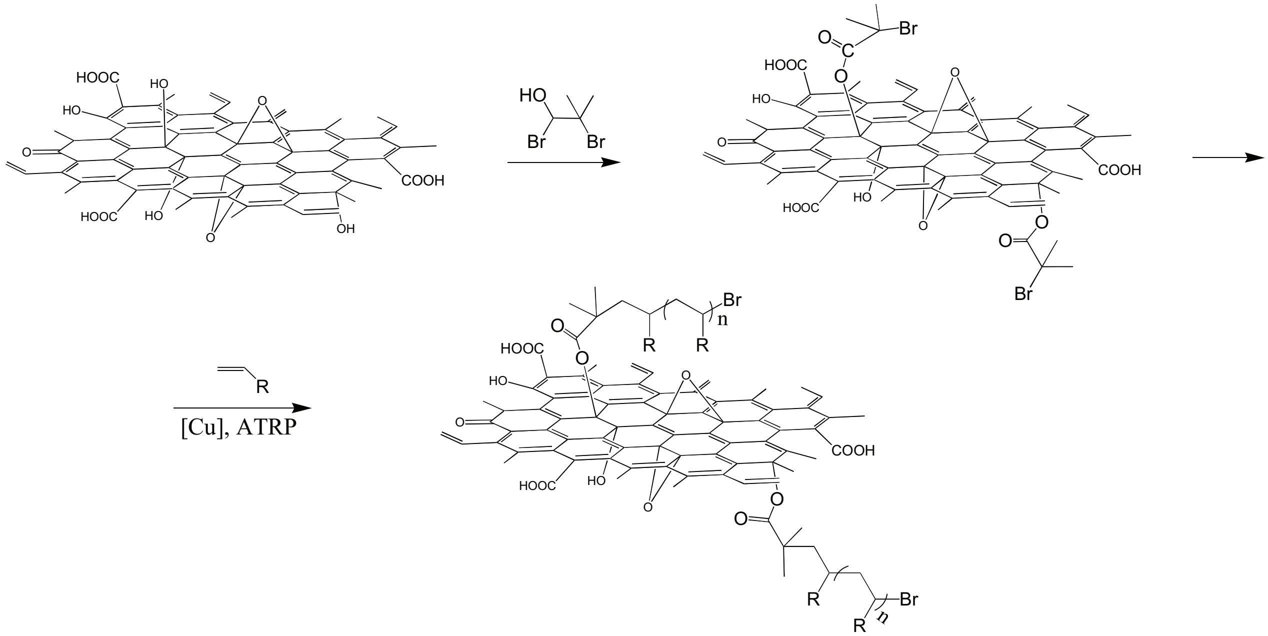

Scheme 4.

curred after the reaction of the isocyanates with –OH and COOH functionalities of graphene sheets were observed by FT-IR spectroscopy. Upon treatment with phenyl isocyanate, the C=O stretching vibration at 1733 cm^{-1} in GO became obscured by the stronger absorption at 1703 cm^{-1} from the carbamate esters. In addition, a new stretching band at 1646 cm^{-1} appeared and was assigned to an amide carbonyl-stretching mode and band at 1543 cm^{-1}, which originated from the C-N stretching vibration of either amides or carbamate esters. The approximate degree of functionalization for various isocyanates was calculated from the carbon to nitrogen atomic ratio as was determined by elemental analysis. The extent of functionalization with various aromatic and aliphatic isocyanates appeared to correlate with their relative reactivities. Depending on the isocyanate structure the degree of functionalization was one carbamate group per 4 to 20 graphene carbons. Because the degree of functionalization could also be controlled by the reaction time, it was possible to prepare GO with only partial isocyanate functionalization and then subject it to a second chemical treatment to functionalize the remaining hydroxyls. In all cases, the AFM images showed the complete exfoliation of the functionalized GO in DMF with platelets that were about 1 nm thick. Such functionalized graphenes formed good dispersions in aprotic polar organic solvents such as DMF, DMSO and N-methylpyrrolidone (NMP). Other solvents, such as THF, toluene, acetone, methylene chloride, methanol and ethanol, did not disperse these materials. On the contrary, Wang *et al.* reported a better dispersibility of graphene, functionalized by reaction with phenylisocyanate, in DMF as well as in nonpolar organic solvents like THF and *n*-hexane [98]. Good exfoliation of the functionalized GO was further used for the preparation of electrically conductive graphene/polystyrene (PS) nanocomposites. The composites were prepared by solution phase mixing of the exfoliated phenyl isocyanate-treated GO with PS followed by their chemical reduction [29]. Such material exhibited a very low percolation threshold of fillers at 0.1 vol% as a consequence of the perfect homogeneous exfoliation and high aspect ratio of individual graphene sheets.

In two works [99,100] the hydroxyl groups of GO were used for a reaction with α-bromoisobutyryl bromide (see Scheme (**4**)). By this approach an atom transfer radical polymerization (ATRP) initiator was covalently bonded to the graphene surface. Such a functionalized graphene was subsequently used as a multifunctional initiator for the polymerization of styrene, butyl acrylate, methyl methacrylate and 2-dimethylaminoethyl methacrylate. For steric reasons this "grafting from" method has advantages for achieving higher and controlled degrees of functionalization in comparison to a "grafting to" method, in which already prepared polymer is reacting with the graphene surface. The attachment of the ATRP initiator was confirmed by XPS, where signals attributed to C-Br bonds

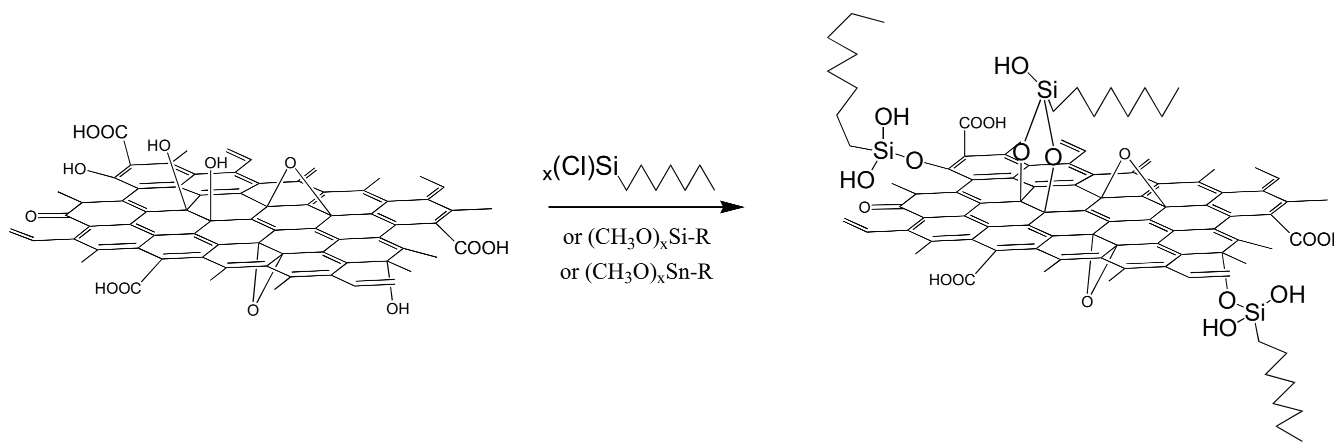

Scheme 5.

emerged and the intensity of the signals attributed to C-O groups diminished after modification. Based on elemental analysis, the functionalized GO materials were calculated to contain 1.2% initiator by weight, corresponding to one initiator per 33 carbons, or 0.115 mmol of initiator per 100 mg of functionalized GO. Because the reaction conditions caused a slight reduction of the oxide functionality present on the surface of GO, powder of the initiator-functionalized GO showed electrical conductivity 100 times higher than that of the starting material. Polymerization of the monomers was performed using a catalyst system consisting of copper wire and tris(2-aminoethyl)amine as a ligand. Analysis of the polymer chains via solution phase ^{1}H NMR spectroscopy verified that the polymerizations from the functionalized GO surfaces were successful for all the investigated monomers. The absolute molecular weights were calculated using end-group analysis. The authors also showed the ability to control the molecular weight of the grafted PS through simple adjustment of the initiator:styrene ratio. TEM and diffraction analysis confirmed exfoliation of polymer-functionalized GO into single layers. The solubility of the polymer-functionalized GO proved to be dependent on the type and chain length of the polymer as well as on the concentration of the composite. PS-functionalized GO was soluble in both polar and relatively nonpolar organic solvents, including DMF, toluene, chloroform and methylene chloride, up to 30 mg.ml^{-1}.

The hydroxyl groups of GO were also used as reaction sites for the silanization of the graphene surface. In two works, Matsuo *et al.* [101,102] showed silane modification of GO with different alkylchlorosilanes in the presence of butylamine and toluene. Only silylating agents with two or three chlorine atoms at silicon ($C_xSiMeCl_2$, C_xSiCl_3) reacted successively with the hydroxyl groups of oxidized graphene to form Si-O bonds (see Scheme (**5**)). No reaction occurred when silylating reagents with only one chlorine atom (C_xSiMe_2Cl) were used. FTIR analysis was used for the structural characterization of the main new bonds formed during silanization. Bands around 2920, 1450, 1115 and 890 cm^{-1} were observed after the reaction of GO with alkylchlorosilanes. In addition to these, peaks at 1270 and 815 cm^{-1} appeared for the sample reacted with $C_xSiMeCl_2$. On the other hand, bands related to water and C-OH band at 1620 and 1380 cm^{-1} became smaller for the silylated samples. Optimization of reaction conditions with respect to both reaction time and amount of butylamine agent was also performed. The role of butylamine in this reaction was to both stabilize the exfoliation of GO against the fast Van der Waals interactions of particular sheets and scavenge HCl molecules, which cause decomposition of silylated GO. It was shown by X-ray diffraction that the interlayer spacing of the silylated GOs obtained increased almost linearly with the corresponding increase in alkyl chain length. The angle 2θ decreased from 14° for GO to 6.5°-6.1° for silylated samples. From the elemental analysis it was determined that the ratio of silylating reagent/GO was almost 0.6 for the samples obtained using C_4SiCl_3, C_8SiCl_3 and $C_{10}SiCl_3$. The content of acidic hydroxyl groups in GO being 0.9-1.2 mol/mol GO unit indicated that one alkyl silane molecule reacted with two hydroxyl groups of GO. Surprisingly, reactions of the silane molecules with longer alkyl chain lengths led to a higher content of silicon on graphene, reaching 1.7 silylating reagents/GO in the case of $C_{18}SiCl_3$. The reason for this effect is not clear, but as a possible explanation the authors noted the effects of intramolecular reactions of GO-bound silicon atoms with adjacent hydroxyl functionalities leading to a bridging effect on the surface.

The modification of GO consisting of 4-6 layers with silane derivatives was also reported by Subrahmanyam *et al.* [103]. In addition to reactions with hexadecyltrimethoxysilane, the hydroxyl groups on the graphene surface were also reacted with dibutyldimethoxytin. Functionalization was confirmed by IR spectroscopy where bands due to the alkyl groups as well as Sn-O or Si-O (1100 cm^{-1}) vibration bands were observed. The functionalized samples were dispersible in CCl_4 and the dispersions were stable for at least 6 hours.

The epoxide is yet another functional group located on the basal plane of graphene sheets in GO that can allow for the functionalization of the graphene surface. Bourlinos *et al.* [82] modified the surface of GO with aliphatic amines and functional amines such as amino acids and aminosiloxanes. Structurally, all modified graphites were strongly evidenced by FTIR and ^{1}H NMR spectroscopies, where strong absorptions below 3000 cm^{-1} and chemical shifts at 0.9 and 1.1 ppm confirmed the presence of aliphatic CH_3- and –CH_2- groups. They showed that the main insertion pathway is a nucleophilic attack of an amine on the epoxy groups of GO (see Scheme (**6**)). XRD proved that the interlayer distance increased with the length of the alkyl substituents of the amines. The basal spacing fit the equation: $d_{001} = 6.1 + l_c\sin\theta$, where 6.1 is the thickness of the GO layers in Å, l_c *is* the length of the hydrocarbon chain of the amine molecule and θ is the hydrocarbon chain inclination. Modification of GO with longer aliphatic amines such as ODA led to an organophilic solid and its dispersion increased in the follow-

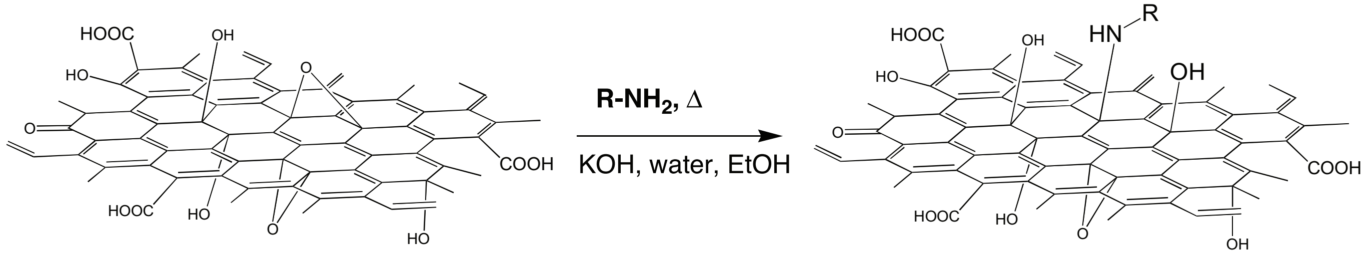

Scheme 6.

ing order: chloroform > THF > toluene, dichlormethane. The basal spacing for GO modified with ODA was d_{001} = 28 Å. Similarly, treatment of the GO with $(CH_3O)_3SiCH_2CH_2CH_2NH_2$ led to an organosilasesquioxane-pillared GO structure with d_{001} = 13.7 Å. In contrast to the aforementioned amine molecules, the insertion of amino acids such as H_2NCH_2COONa and $H_2N(CH_2)_7COONa$ induced only small changes in the basal spacing of GO irrespective of their chain length, even though the covalent bonding of the amine groups to the GO surface was confirmed. The authors suggested that the amino acid molecules adopt a flat orientation in the interlayer zone of GO due to the hydrogen bonding interactions of the carboxylate groups of the grafted amino acids with oxygen containing groups of GO. On the other hand, such modified GOs formed aqueous colloidal dispersions. The addition of $C_{16}H_{33}N(CH_3)_3^+Cl^-$ led to ionic bonding of the ammonium ion with the carboxylate of the modified GO as observed by a sharp reflection in the XRD at d_{001} = 37 Å, characteristic of a bilayer arrangement of the surfactant cations within the interlayer space of the modified solid.

The aforementioned study was completed by Herrera-Alonso *et al.* [104], who investigated the modification of GO with diaminoalkanes (n = 4 – 10). A gradual increase in the basal spacing of GO was observed as the hydrocarbon chain length of the diamine increased from butane to decane, suggesting that intercalation takes place and the interlayer spacing was sensitive to the size of the intercalant. However, the interlayer spacing of GO modified with diaminoalkanes did not reflect the values of an interlayer spacing of GO modified with monoaminoalkanes with the same number of methylene groups. Finally, it was demonstrated that the reaction of GO with diaminoalkanes under reflux for extended periods (>72 hours) resulted in the chemical reduction of the GO to a disordered graphitic structure. The presence of new groups on graphene was followed by FTIR spectroscopy. New bands appeared in the FTIR spectra at 1470, 1570, 2924 and 2852 cm^{-1} and were attributed to the bending vibrations of $–CH_2$- and –N-H groups and the asymmetric and symmetric vibrations of methylene groups, respectively. The positions of both the diaminooctane modified GO bending vibration at 1467 cm^{-1} and asymmetric vibration at 2929 cm^{-1} can be used to establish the chain conformation (*gauche/trans* ratio). Higher frequencies are indicative of all-*trans* chains.

The ring-opening reaction of the epoxy groups of GO catalyzed by potassium hydroxide was also used for ionic-liquid functionalization of graphene sheets with 1-(3-aminopropyl)-3-methylimidazolium bromide [105,106]. The characteristic asymmetric stretching absorption bands of the imidazolium ring in FTIR spectra were found at 1164 cm^{-1}. The electronic conjugation of graphene was proved using UV-Vis spectroscopy following red band shifts from 230 nm to 260 nm for graphene before and after the reduction procedure. Functionalized GO was well dispersed in water, DMF and DMSO due to an enhanced solubility and electrostatic inter-sheet repulsion provided by the ionic liquid units. The authors reported that the dispersions were stable for more than three months while it was proved that good exfoliation was obtained. The final material after reduction of the residual oxygen groups was immobilized onto chitosan film on the surface of glassy carbon electrodes. The electrode was then used as a sensor for ethanol through an NADH amperometric response.

Modification of the graphene surface of GO by ODA was described in another two works [107,108]. Functionalized GO could be exfoliated to give dispersions in THF, toluene, DMF, cyclohexane, chlorobenzene and dichloromethane, which were stable for more than 6 months. Covalent functionalization was confirmed by FTIR, where asymmetric vibrations of the methylene group at 2874 and 2918 cm^{-1} were observed. Similarly, N-H vibrations observed at 1468 cm^{-1} confirmed the modification, as well. The functionalized GO was subsequently reduced by heating. Elemental analysis and FTIR confirmed that two–thirds of the oxygen and one-half of the alkyl chains were lost by heating at 300°C. The conductivity of the GO films was also reported [107]. The annealing of the film of functionalized GO at 300°C led to a rapid rise in conductivity from less than 10^{-7} S cm^{-1} to 10 S cm^{-1}.

Wang *et al.* [98] modified GO by thermal treatment of GO/water dispersions with allylamine/ethanol mixtures in an autoclave. Such processing led to the enhanced water solubility of graphene from 0.69 mg ml^{-1} to 1.55 mg ml^{-1}.

2.3.2. Reactions on Aromatic Rings of Graphene Sheets

One possible way of functionalizing graphene aromatic rings is by substitution of metalized graphite. Chattopadhyay *et al.* [109] described an electrophilic substitution of the lithium graphite with *n*-dodecyl iodide for the preparation of exfoliated soluble graphite. The C-Li bond was first introduced onto graphite by treatment of graphite with lithium metal in the presence of ammonia under an argon atmosphere according to Scheme (**7**). Subsequently, the addition of *n*-dodecyl iodide led to the covalent hydrophobization of graphite by *n*-dodecyl chains. Covalent attachment of the dodecyl radicals was demonstrated by Raman spectroscopy, where the D band of the functionalized material at 1299 cm^{-1} was enhanced as a result of the chemical disruption of the sp^2 hybridized carbon atoms of the graphite. In addition, C-H stretching bands associated with the dodecyl groups at 2917 and 2840 cm^{-1} were observed in the FT-IR spectra. Elemental analyses showed that while starting graphite gave less than 0.05% hydrogen, graphite recovered after the reaction with lithium in liquid ammonia without the dodecyl iodide had 1.7% hydrogen and dodecylated graphite contained 2.25% hydrogen. A series of standard analyses, such as AFM and XRD, was used to determine the bulk properties of prepared exfoliated graphite and showed irregular modified graphite nanoplatelets with a height of 3.5 nm.

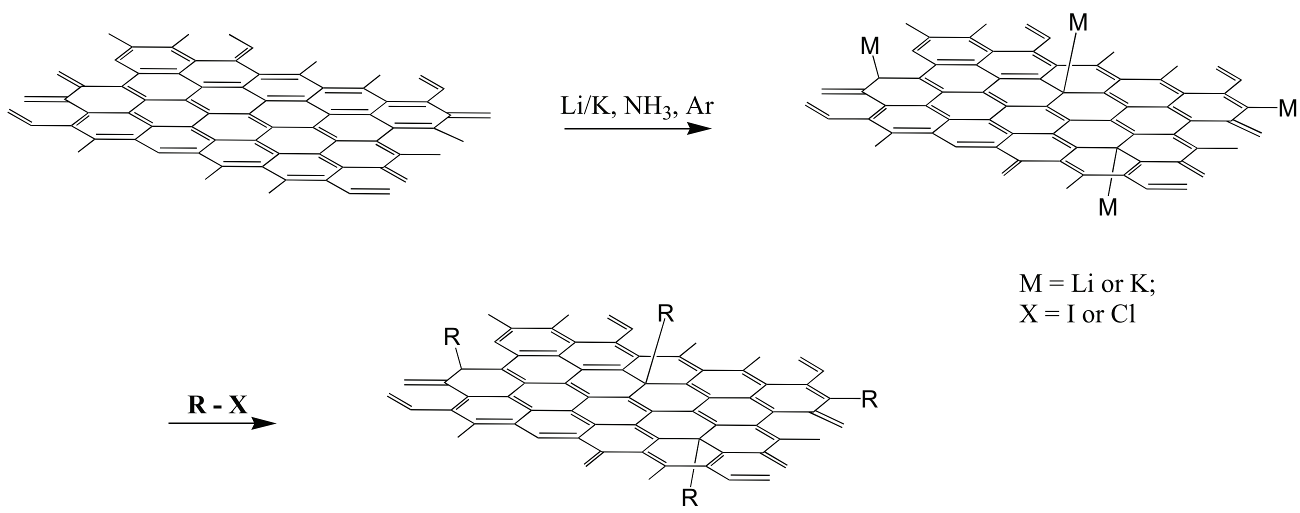

Scheme 7.

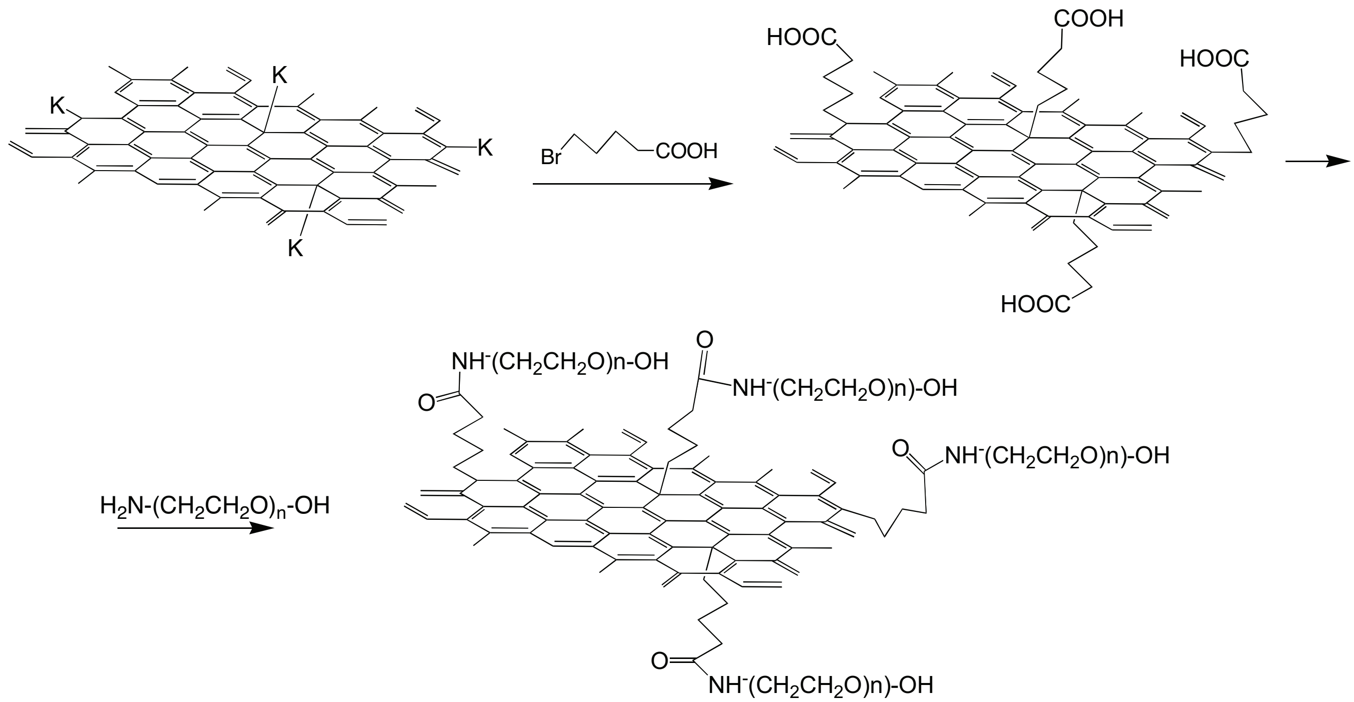

Scheme 8.

Another type of metalized graphite, potassium graphite, was used in the reaction with 1-iodododecane to produce dodecylated graphite (see Scheme (**7**)) [110]. The FT-IR spectra confirmed the presence of C-H stretching bands at 2800-3000 cm^{-1} associated with the dodecyl groups. TGA indicated a weight loss of 15%, which corresponds to about one dodecyl group per 78 graphite carbon atoms. Prepared dodecylated graphite was soluble in chloroform, benzene and 1,2,4-trichlorobenzene. Moreover, its solubility in water was achieved by the reaction of potassium graphite with 5-bromovaleric acid and subsequent reaction with amine-terminated PEG (see Scheme (**8**)). The FT-IR spectra of acid functionalized graphite showed a broad hydroxyl absorption at 3400 cm^{-1} and a sharp carbonyl absorption at 1678 cm^{-1}. After reaction with PEG the carbonyl group was shifted to 1624 cm^{-1} and the N-H stretching band was found at 3738 cm^{-1}, in accordance with amide bond formation. XPS of PEGylated graphite showed the presence of distinct C1s, O1s, and N1s peaks at 284.6, 533, and 400.2 eV, respectively. The TGA of acid functionalized graphite indicated a weight loss of 12%, corresponding to one $C_4H_8CO_2H$ group per 61 graphite carbon atoms. AFM images showed that graphite functionalized with PEG chains had height between 2-9 nm.

Bon *et al.* [111] used plasma assisted decomposition of CF_4 to prepare fluorinated graphene sheets. Subsequently, the fluorinated graphene sheets were dispersed in butylamine and sonicated for 1 hour. During this treatment butylamine was attached to the graphene sheets through an elimination of the fluorine atoms and formation of C-NHR bonds (see Scheme (**9**)). The authors used IR spectroscopy to verify the transformation. After the plasma treatment, a band at 1260 cm^{-1} was observed and attributed to covalent C-F bonding. Similarly, in the XPS spectra a peak at 290.1 eV characteristic of C-F bonds was found after treatment with CF_4. During the subsequent reaction with a butylamine, the asymmetric and symmetric stretching vibrations of the primary butylamine at

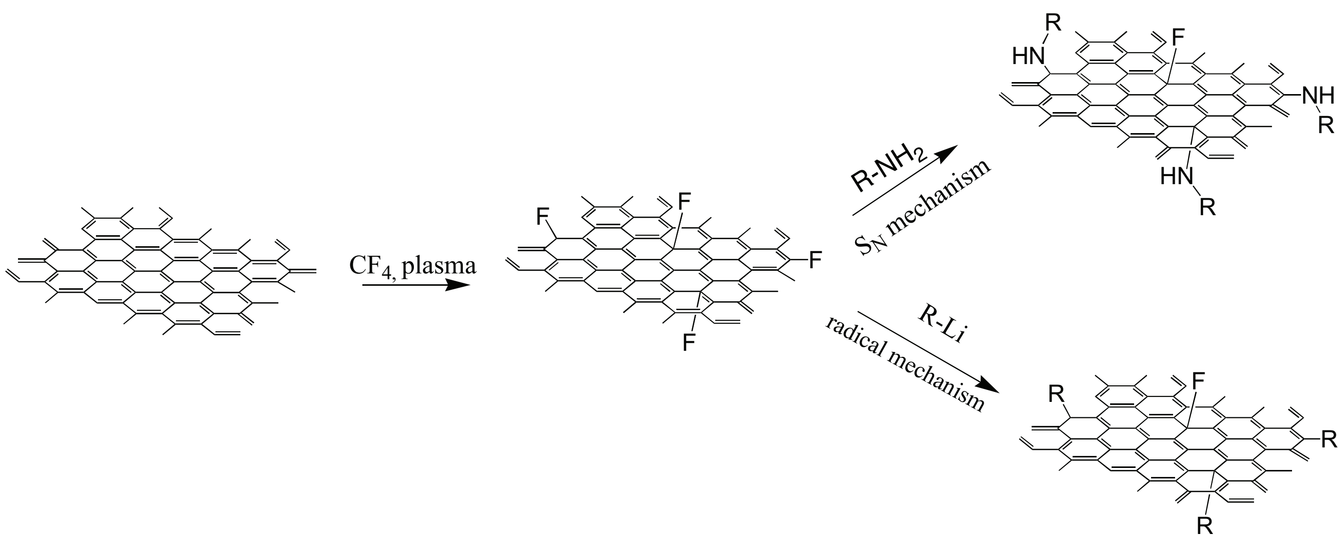

Scheme 9.

3290 and 3370 cm^{-1}, respectively, disappeared and a broad band at 3400 cm^{-1}, attributed to a secondary amine, appeared in the IR spectra. Moreover, a band at 1260 cm^{-1}, attributed to a covalent C-F bond, disappeared after the reaction. In the XPS spectra a N1s peak was observed in the butylamine functionalized graphene. A peak fitting procedure reveals two N1s components with binding energies of 399.5 and 400.5 eV, corresponding to NH_2 and NH groups, respectively. Amino-functionalized graphene was well dispersed in organic solvents. AFM images showed the graphene sheets with average thickness of 0.7-0.9 nm, which is characteristic of exfoliated graphene sheets.

A high level of functionalization of fluorinated graphite with dodecyl groups was reported by Chakraborty *et al.* [112]. During this functionalization, a carbon-centered free radical was formed after electron transfer from lithium to the fluorinated graphite and subsequent decomposition of the transient radical anion formed (see Scheme (**9**)). This carbon-centered radical was then reacted with a dodecyl radical originating from the radical anion of dodecyl iodide, which was formed after a similar electron transfer process. After the functionalization, the white fluorinated graphite changed color to black, indicating that the fluorine groups were replaced by dodecyl functionalities. In the Raman spectra the dodecylated graphite exhibited a G band at 1590 cm^{-1} and a D band at 1290 cm^{-1} that arose from covalent attachment of the dodecyl groups. The D/G ratio was 2:1, indicating a high level of functionalization. During the alkylation the FT-IR spectra showed a disappearance of the C-F stretching absorptions between 1072 and 1342 cm^{-1} and an appearance of the C-H stretching bands from the dodecyl groups at 2800-3000 cm^{-1}. XPS confirmed that nearly all of the fluorine atoms were displaced by the dodecyl functionalities. The TGA showed a 40% weight loss, indicating that the functionalized graphite had one dodecyl group per 21 graphitic carbon atoms. This was about a 3 times higher functionalization than was reported by the same authors for dodecylated graphite prepared from potassium graphite [110]. The functionalized material was soluble in chloroform, dichloromethane, DMF, DMSO, benzene and 1,2,4-trichlorobenzene. The solubility in chloroform was determined to be as high as 1.2 $g.l^{-1}$. The AFM image of the dodecylated graphite showed that the average height was between 2 – 12 nm.

Worsley *et al.* [113] used graphite fluoride for alkylation reaction with alkyl lithium reagents such as butyl and hexyl lithium in the presence of tetramethylethylenediamine. The authors showed that the alkyl lithium reagent both replaces fluorine by alkyl groups and introduces additional double bonds by eliminating molecular fluorine. This was confirmed by FT-IR spectroscopy, where in addition to the C-H stretching bands of the alkyl groups at 2850-3000 cm^{-1} bands were also observed at 1450-1600 cm^{-1}, which can be attributed to C=C stretching. The alkylated graphene was dispersible in THF and in halogenated solvents such as dichlorobenzene and dichloromethane. The solubility was dependent on the degree of alkylation of the graphene sheets. Using near IR the authors determined that the solubility of the best soluble butylated and hexylated graphene sheets in THF was 0.24 and 0.54 $g.l^{-1}$, respectively. It was found in AFM images that the average thickness of such functionalized graphene layers was 0.95 nm. In height mode of the AFM images the roughness of the nanoplatelets was also visible, as is expected for graphene that is highly functionalized in the basal plane. The authors attributed the variability in the height to the local degree of functionalization, with high points in the areas where the functionalization is especially dense and the hexyl groups are standing perpendicular or at a substantial angle to the graphene plane.

Another method, which does not require an oxidized graphene surface (more to the contrary, its efficiency is higher in non-oxidized or reduced graphene sheets) is functionalization by diazonium salts (see Scheme (**10**)). Bekyarova *et al.* [114] demonstrated the chemical modification of epitaxial graphene by covalent attachment of nitrophenyl groups to the basal carbon atoms. The surface modification was achieved through an electron transfer from the graphene layer to the diazonium salt and its subsequent spontaneous reaction with the graphene surface. The presence of nitro groups on the graphene surface was confirmed by FT-IR spectroscopy, because the nitrophenyl functionalized graphene exhibited new bands at 1565 and 1378 cm^{-1}, corresponding to the symmetric and asymmetric stretching bands of the nitro group. In addition, the XPS spectrum showed a peak at 406.36 eV that was assigned to the nitro groups. Cyclic voltammetry was used to estimate the surface coverage of the nitrophenyl groups. The surface coverage was about 1×10^{15} $molecules.cm^{-2}$ of graphene sheet, which was in good agreement with the theoretical coverage of 5×10^{14} $molecules.cm^{-2}$ based on an ideal, fully ordered close-packed monolayer of vertically oriented nitrophenyl groups. Based on the XPS, the nitrophenyl groups were present on the graphene surface even after heat-

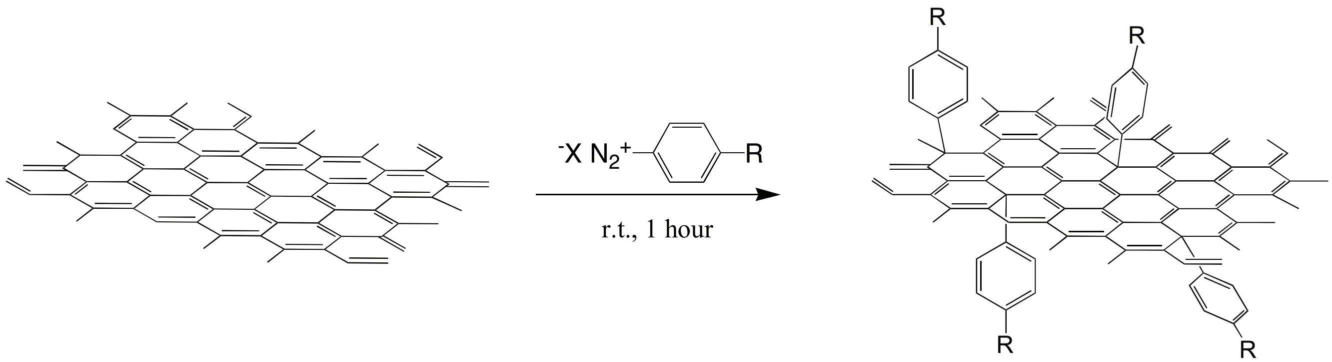

Scheme 10.

ing at 200°C in a vacuum for 2 hours. The authors also showed that the modification of graphene sheets led to a more than double increase in the room temperature resistance (from 1.5 kΩ.cm^{-2} to 4.2 kΩ.cm^{-2}), thus suggesting a change in the electronic structure and transport properties of graphene from near-metallic to semiconducting. The functionalized graphene surface was further used as a working electrode and the nitro groups were reduced to amine groups in aqueous solution as confirmed by XPS, where a single peak at 399.30 eV was observed.

Lomeda *et al.* [115] reported the diazotation of graphene sheets using chlorophenyl, bromophenyl, nitrophenyl and methoxyphenyl diazonium salts in the presence of surfactants under basic conditions. To achieve good exfoliation, graphite was first oxidized to GO. In the next step the dispersed GO was reduced by hydrazine and subsequently functionalized. The ATR-IR spectrum of graphene functionalized with nitrobenzene groups showed the asymmetric and symmetric stretches of the nitro group at 1513 and 1343 cm^{-1}, respectively, in addition to C-N stretches at 852 cm^{-1}. The presence of nitro groups was also confirmed by XPS with a strong signal at 406 eV. Similarly, XPS was used to confirm the functionalization of graphene with halogen derivatives. The atomic percentages of halogens estimated by XPS were 4.6% Cl and 3.2% Br for chlorobenzene and bromobenzene derivatives, respectively. It was also proved that diazonium functionalization was more efficient after the reduction of oxidized graphene sheets. The degree of functionalization for all derivatives was estimated from TGA to be about 1 functional group per 55 carbons. The functionalized graphene was readily dispersed in DMF, DMAc and NMP and the solubility in DMF was established to be 0.25-0.5 mg.ml^{-1} depending on the aryldiazonium derivative. AFM showed single or bilayers of graphene sheets. Diazonium functionalization was also used in the preparation of water-soluble graphene after its reduction from GO.

Diazonium salts were also used for introducing sulfonic acid groups onto the graphene structure [116]. The functionalization was carried out on GO partially reduced by $NaBH_4$. Elemental analysis showed that while modification of unreduced GO via diazonium salts gives a S:C ratio of only 1:148, after prereduction of GO the ratio can be increased to 1:35 under the same reaction conditions. The ATR-IR spectra of sulfonated graphene showed the presence of peaks at 1175, 1126 and 1040 cm^{-1} from sulfonic acid groups and peaks at 1007 and 830 cm^{-1} characteristic of vibrations from a *p*-disubstituted phenyl group. Charged $-SO_3^-$ units prevented the graphitic sheets from aggregating in solution after the subsequent second reduction stage of the GO by hydrazine. Such an approach allowed the preparation of isolated sheets of lightly sulfonated graphene with improved water solubility of about 2 mg.ml^{-1} in the pH range of 3-10. Isolated sulfonated graphene sheets could also persist in the mixture of water and organic solvents including methanol, acetone and acetonitrile, making it amenable to further modification. The conductivity of the final reduced sulfonated graphene was 1250 S.m^{-1}, which is about 4-times lower than that for neat graphite. A similar procedure but which also includes a second sulfonation step was used for the preparation of highly sulfonated graphene [117]. The presented sulfonyl groups were used as doping groups for poly(3,4-ethyldioxythiophene) (PEDOT) to enhance the conductivity and mechanical properties of graphene/PEDOT hybrid materials.

To develop high performance, graphene-based nanocomposites, the addition of diazonium salts onto graphene nanosheets was done to enable the covalent bonding of ATRP initiators onto the graphene surface [118]. Subsequent atom transfer radical polymerization allowed for the linking of PS chains to the graphene nanosheets. Functionalization of the graphene surface was clearly supported by an increase in the D/G bands ratio at 1333 and 1582 cm^{-1}, respectively, in Raman spectra expressing sp^3/sp^2 carbon ratios. Further evidence of covalent bonding between graphene and PS chains is provided by the Fourier transform infrared (FT-IR) spectra. The FT-IR spectrum from the initiator-grafted graphene sheets exhibited two peaks at 1740 and 1160 cm^{-1} that are characteristic of ester bonds. In FT-IR spectra of PS-grafted graphene, four strong peaks at 700, 754, 1480 and 1490 cm^{-1}, corresponding to absorptions of the benzene ring of PS segments, and peaks at 2920 and 3030 cm^{-1} from the methylene groups were observed. The prominent confinement effect arising from nanosheets resulted in a 15°C increase in the glass transition temperature of PS compared to that of the pure polymer. The resulting PS nanocomposites with 0.9 wt% graphene nanosheets revealed around 70% and 57% increases in tensile strength and Young's modulus.

Choi *et al.* [119] reported the functionalization of epitaxial graphene via nitrene radicals formed by the thermal decomposition of azidotrimethylsilane (see Scheme (**11**)). After removing N_2, the nitrene can react with graphene via both electrophilic cycloaddition reactions and biradical pathways after intersystem crossing. However, it was found that the efficiency is quite low, as just one nitrogen per 53 carbons was found. The authors used high resolution photoemission spectroscopy (HRPES) to confirm a covalent functionalization of the graphene surface. By observing the bonding nature of the N 1s peaks, they found that two distinct N peaks can be clearly distinguished in the spectra at 398.5 and 399.7 eV. Using a covalently bound, stretched graphene (CSG) model, they elucidated that nitrene radicals were adsorbed on the graphene layer at

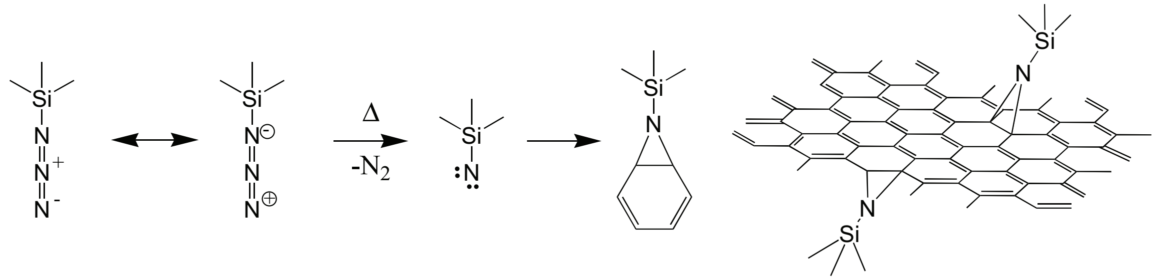

Scheme 11.

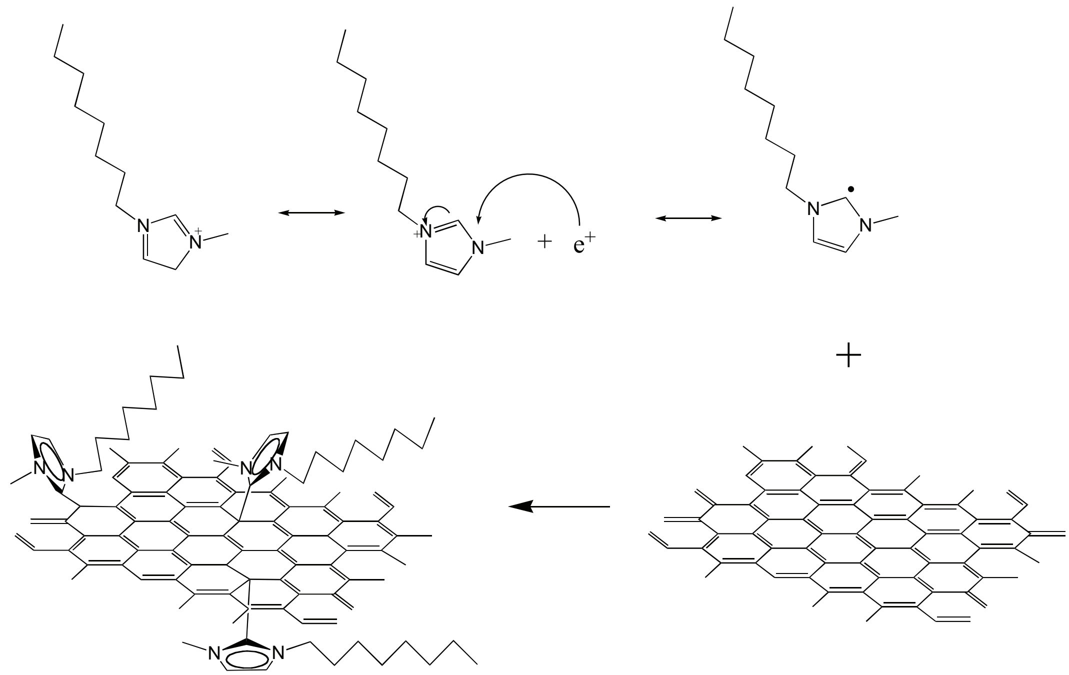

Scheme 12.

two different adsorption sites. The successful functionalization of *ortho*-dichlorobenzene (OCDB)-dispersed graphene by thermal decomposition of aryl azides was also mentioned in the work of Hamilton *et al.* [120], but the authors did not give more information. The same authors also mentioned the successful functionalization of OCDB-dispersed graphene by radical addition of alkyl iodides. This addition was initiated by the thermal decomposition of benzoyl peroxides. The authors indicated that more details on this functionalization would be published.

An electrochemical approach to graphene surface functionalization was used for the preparation of ionic-liquid-functionalized graphite sheets, which could be exfoliated into functionalized graphene nanosheets [121]. As an ionic liquid, various 1-octyl-3-methyl-imidazolium salts with different types of anions were used. It was suggested that during the electrochemical reaction process an electron transfer to the ionic liquid occurred. According to semiempirical calculations, the unpaired electron was located mainly on the C2 carbon of the imidazolium ring of the ionic liquid. Reduction of the cation led to the formation of the 1-octyl-3-methylimidazolium free radical, which could combine with one of the electrons of the π-bond of the graphene (see Scheme (**12**)). The connection of ionic liquids to the graphene surface was verified by XPS and FTIR spectroscopy. In XPS, a well defined peak at 399.84 eV was observed, consisting of two modes at 399.80 and 401.51 eV from two different types of nitrogen atoms of the imidazolium ion connected to graphene surface. FT-IR analysis showed the presence of C-H stretching bands at 2923 and 2853 cm^{-1}, a C-H vibration at 1454 cm^{-1} as well as the imidazolium framework vibration at 1616 cm^{-1}. Due to the hydrophobic groups attached to the graphene surface, the obtained modified graphene nanosheets readily formed stable and homogeneous dispersions in polar aprotic solvents such as DMF, DMSO and NMP solutions after sonication. In DMF the AFM revealed exfoliated graphene with an average thickness ca. 1.1 nm. The authors also investigated the influence of ionic liquids on the electrical conductivity of modified graphene nanosheets/PS composites. The results indicated that the anion does indeed have a crucial effect on the conductivity of modified graphene nanosheets. The best conductivity was found for graphene modified by 1-octyl-3-methyl-imidazolium hexafluorophosphate with a percolation threshold of 0.1 vol % and a conductivity of 13.8 S.m^{-1} at a 4.19 vol % modified graphene content.

A simple method for the covalent functionalization of graphene by a polymer chain is the grafting of polymer radicals onto the graphene surface (see Scheme (**13**)). Poly(acrylic acid) (PAA) and polyacrylamide (PAM) were grafted to the surface of reduced GO in a water suspension using ammonium peroxosulfate as an initiator of the acrylic acid and acrylamide monomers [122]. Raman and FT-IR spectroscopy were used for structural characterization of the modified samples. Raman spectroscopy is strongly sensitive to the electronic structures of samples and can thus be used for observing

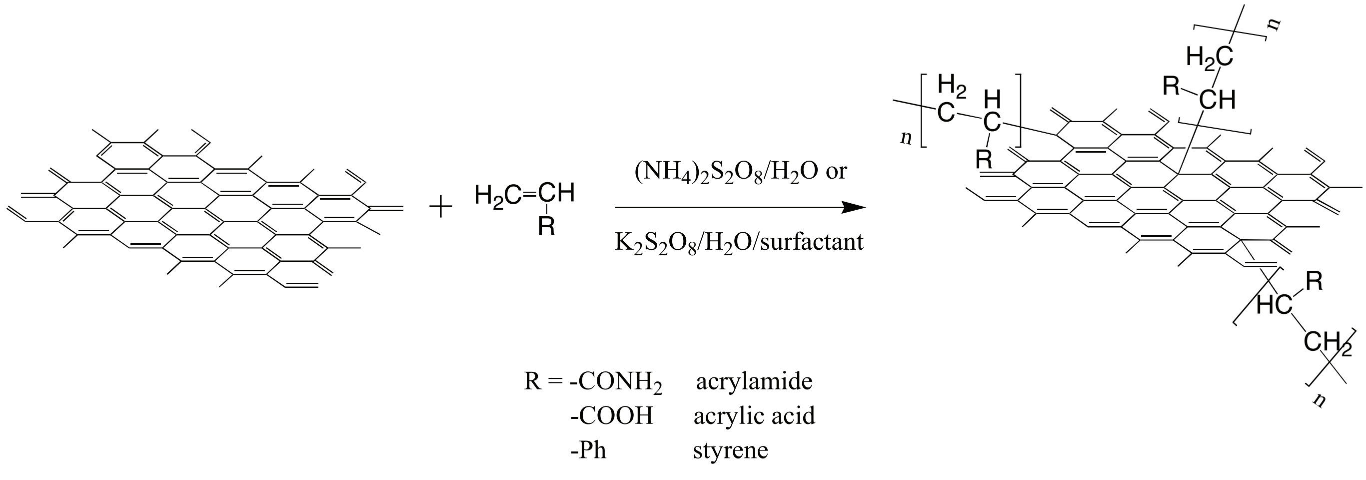

Scheme 13.

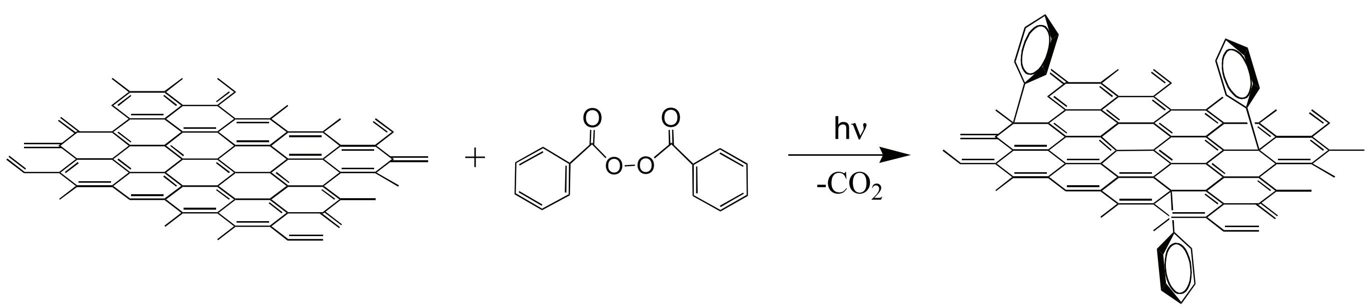

Scheme 14.

the newly formed sp^3 hybridized carbons of graphene after the grafting of a monomer (macromer). Comparing the data with that for raw graphite, the ratios of the intensities of the D band at 1330 cm^{-1} and G band at 1580 cm^{-1} for both types of modified graphene were markedly increased, indicating the formation of the sp^3 carbon after functionalization. FTIR only confirmed the presence of a carbonyl stretching vibration at 1720cm^{-1} and a C-H stretch at 2960 cm^{-1}. TGA gave 82% and 65% weight loss of the organic part for PAA-g-graphene and PAM-g-graphene, respectively. This corresponded to composites containing graphene nanoplatelets and PAA or PAM with weight ratios of 2:9 or 1:2. The same authors reported the preparation of graphene nanoplatelets grafted by PS-b-PAM block copolymers [123]. In this case the TEMPO-terminated PS macroinitiator was prepared first and then mixed and heated with reduced GO, acrylamide and benzoyl peroxides to start the synthesis of block copolymers for grafting to graphene surfaces. The final composite contained graphene and PS-b-PAM in a 1:4 ratio. In both works the authors reported the average thickness of the graphene nanoplatelets of 1.2 nm, which could correspond to exfoliated single layers and up to 3 graphene layers.

Unlike previous cases where the authors first reduced GO and then performed grafting of the polymers, Hu *et al.* [124] first reported grafting of GO and its immediate subsequent reduction. The grafting was carried out using an emulsion radical polymerization of styrene in the presence of SDS as a surfactant and potassium peroxosulfate as an initiator. The formation of micelles on the graphene edges was reported as a consequence of interactions between oxygen-containing hydrophilic groups and surfactant, while the other micelles were dispersed in the interface media through dynamic equilibrium. Such adsorbed micelles then acted as the base for covalent linking of PS onto graphene. The final material consisted of PS microspheres covalently linked to the edges of reduced graphene nanoplatelets. The presence of PS was confirmed by FTIR because typical PS absorption vibrations at 3028, 2921, 1605, 1493, 1450 and 1029 cm^{-1} were observed. Raman spectroscopy was used to show the higher order possibilities for the grafting reaction on sp^3 carbons, as the I(D)/I(G) ratio of bands at 1331 and 1594 cm^{-1} was 1.156. The PS-graphene composite was dispersible in toluene and chloroform and the suspensions were stable for more than 4 months. The electrical conductivity of PS with 2 wt% graphene was 2.9×10^{-2} $S.m^{-1}$.

Liu *et al.* [125] reported the photochemical functionalization of graphene sheets. It was found that benzoyl peroxides decomposed in the presence of graphene when irradiation was applied (see Scheme (**14**)). As a result, a phenyl radical decomposition product, formed by decarboxylation of benzoyloxyl radicals, was bound to the graphene surface. The mechanism was studied and it was suggested that benzoyl peroxide accepts a hot electron from photoexcited graphene, which serves as a sensitizer. The benzoyl peroxide radical anion then spontaneously decomposes to benzoate and the benzoyloxyl radical. The hot electron transfer mechanism is consistent with the observation of a strong dependence of the reaction kinetics on the excitation energy. An increase in the excitation energy increased the energy of the hot electron and thus increased the rate of electron transfer to benzoyl peroxide. Single-layer graphene was about 14 times more reactive than was double layer graphene. During the functionalization a significant sp^3 defect in the basal plane of graphene was produced, as was confirmed by Raman spectra in which a strong D band appeared at 1343 cm^{-1}. At the same time the electrical conductivity of the graphene flakes decreased while the hole-doping level increased.

In addition to all the methods of graphene surface functionalization mentioned, a hydrogenation of graphene sheets was reported, as well. Hydrogenation introduces new reactive sites onto the graphene structure and has a significant influence on electrical properties. Moreover, hydrogenated graphene is interesting for its predicted magnetism. Ryu *et al.* [126] reported a reaction of graphene with hydrogen atoms generated during electron beam-initiated crosslinking of a hydrogen silsesquioxane film coated on the graphene sample. The hydrogenation process was followed by Raman spectroscopy based on the appearance of a D-band at ~1350 cm^{-1} induced by local basal plane derivatizations that create sp^3 distortions. It was found that the reaction was significantly faster for single-layer graphene than for double layers. This enhanced reactivity was attributed to the lack of π-stacking and out-of-plane deformation needed to stabilize the transition state of the hydrogenation reaction. The authors also reported that the hydrogenation process can be reversed by photothermal heating under ambient oxygen. The dehydrogenated graphene was activated on SiO_2 and exhibited enhanced chemical doping. Similarly, a reversible hydrogenation of graphene was reported by Elias *et al.* [127] by the reaction of graphene with atomic hydrogen, transforming the highly conductive semimetal into an isolator. The original metallic state was restored by annealing.

3. CONCLUSIONS

In the present review we mentioned the development of many reaction pathways for the covalent modification of graphene. The reactions were divided into two basic parts. The first part was related to the oxidation to GO and following transformation to graphene. The second part covered surface modifications of graphene and was separated into two sub-chapters: the organic chemistry of the functional groups of GO and the surface chemistry of the aromatic rings of graphene. The modifications of graphene significantly affected the solubilities and conductivities of the final materials. These reactions show us one of the possible ways to achieve a high volume production of graphene from a naturally occurring material – graphite.

4. ACKNOWLEDGEMENTS

This work was supported by European Reintegration Grant FP7-ERG-213085 "ORITUPOCO". The authors also thank for the financial support to the Centre for materials, layers and systems for applications and chemical processes under extreme conditions Stage II supported by the Research & Development Operational Programme funded by the ERD and the Grant Agency VEGA through Grant 2/0074/10.

REFERENCES

[1] Radushkevich, L. V.; Lukyanovich, V. M. O strukture ugleroda, obrazujucegosja pri termiceskom razlozenii okisi ugleroda na zeleznom kontakte. *Zur. Fis. Chim.* **1952**, *26*, 88-95.

[2] Kroto, H. W.; Heath, J. R.; O'Brien, S. C.; Curl, R. F.; Smalley, R. E. C60: Buckminsterfullerene. *Nature* **1985**, *318*, 162-163.

[3] Iijima, S. Helical microtubules of graphitic carbon. *Nature* **1991**, *354*, 56-58.

[4] Katsnelson, M. I. Graphene: carbon in two dimensions. *Mater. Today* **2007**, *10*(1-2), 20-27.

[5] Taghioskoui, M. Trends in graphene research. *Mater. Today* **2009**, *12*(10), 34-37.

[6] Steurer, P.; Wissert, R.; Thomann, R.; Mulhaupt, R. Functionalized graphenes and thermoplastic nanocomposites based upon expanded graphite oxide. *Macromol. Rapid Commun.* **2009**, *30*(4-5), 316-327.

[7] Novoselov, K. S., Geim, A.K., Morozov, S.V., Jiang, D., Zhang, Y., Dubonos, S.V., Grigorieva, I.V., Firsov, A.A. Electric field effect in atomically thin carbon films. *Science* **2004**, *306*, 666-669.

[8] Lee, C.; Wei, X.; Kysar, J. W.; Hone, J. Measurement of the elastic properties and intrinsic strength of monolayer graphene. *Science* **2008**, *321*, 385-388.

[9] Subrahmanyam, K. S.; Vivekchand, S. R. C.; Govindaraj, A.; Rao, C. N. R. A study of graphenes prepared by different methods: characterization, properties and solubilization. *J. Mater. Chem.* **2008**, *18*, 1517-1523.

[10] Novoselov, K. S.; Geim, A. K.; Morozov, S. V.; Jiang, D.; Katsnelson, M. I.; Grigorieva, I. V.; Dubonos, S. V.; Firsov, A. A. Two-dimensional gas of massless Dirac fermions in graphene. *Nature* **2005**, *438*(10), 197-200.

[11] Wang, X.; Linjie, Z.; Müllen, K. Transparent, Conductive Graphene Electrodes for Dye-Sensitized Solar Cells. *Nano Lett.* **2008**, *8*(1), 323-327.

[12] Vivekchand, S. R. C.; Rout, C. S.; Subrahmanyam, K. S.; Govindaraj, A.; Rao, C. N. R. Graphene-based electrochemical supercapacitors. *J. Chem. Sci.* **2008**, *120* (1), 9-13.

[13] Stoller, M. D.; Park, S.; Zhu, Y.; An, J.; Ruoff, R. S. Graphene-based ultracapacitors. *Nano Lett.* **2008**, *8*(10), 3498–3502.

[14] Ao, Z. M.; Yang, J.; Li, S.; Jiang, Q. Enhancement of CO detection in Al doped graphene. *Chem. Phys. Lett.* **2008**, *461*(4-6), 276-279.

[15] Leenaerts, O.; Partoens, B.; Peeters, F. M. Adsorption of H_2O, NH_3, CO, NO_2, and NO on graphene: A first-principles study. *Phys. Rev. B* **2008**, *77*(12), 125416.

[16] Schedin, F.; Geim, A. K.; Morozov, S. V.; Hill, E. W.; Blake, P.; Katsnelson, M. I.; Novoselov, K. S. Detection of individual gas molecules adsorbed on graphene. *Nat. Mater.* **2007**, *6*, 652-655.

[17] Jung, I.; Dikin, D. A.; Park, S.; Cai, W.; Mielke, S. L.; Ruoff, R. S. Effect of water vapor on electrical properties of individual reduced graphene oxide sheets. *J. Phys. Chem. C* **2008**, *112,* 20264-20268.

[18] Wehling, T. O.; Novoselov, K. S.; Morozov, S. V.; Vdovin, E. E.; Katsnelson, M. I.; Geim, A. K.; Lichtenstein, A. I. Molecular doping of graphene. *Nano Lett.* **2008**, *8*(1), 173-177.

[19] Ang, P. K.; Chen, W.; Thye, A.; Wee, S.; Loh, P. K. Solution-gated epitaxial graphene as ph sensor. *J. Am. Chem. Soc.* **2008**, *130*(44), 14392-14393.

[20] Wang, Y.; Li, Y.; Tang, L.; Lu, J.; Li, J. Application of graphene-modified electrode for selective detection of dopamine. *Electrochem. Commun.* **2009**, *11*(4), 889-892.

[21] Wang, Z.; Liu, S.; Cai, C. Detection of glucose based on direct electron transfer reaction of glucose oxidase immobilized on highly ordered polyaniline nanotubes. *Analyt. Chem.* **2009**, *81*(4), 1638-1645.

[22] Kang, X.; Wang, J.; Wu, H.; Aksay, I. A.; Liu, J.; Lin, Y. Glucose Oxidase–graphene–chitosan modified electrode for direct electrochemistry and glucose sensing. *Biosens. Bioelectr.* **2009**, *25*(4), 901-905.

[23] Robinson, T. J.; Perkins, F. K.; Snow, E. C.; Wei, Z.; Sheehan, P. E. Reduced graphene oxide molecular sensors. *Nano Lett.* **2008**, *8*(10), 3137-3140.

[24] Sakhaee-Pour, A.; Ahmadian, M. T.; Vafai, A. Potential application of single-layered graphene sheet as strain sensor. *Solid State Commun.* **2008**, *147*, 336-340.

[25] Shan, C.; Yang, H.; Song, J.; Han, D.; Ivaska, A.; Niu, L. Direct Electrochemistry of glucose oxidase and biosensing for glucose based on graphene. *Analyt. Chem.* **2009**, *81*(6), 2378-2382.

[26] Blake, P.; Brimicombe, P. D.; Nair, R. R.; Booth, T. J.; Jiang, D.; Schedin, F.; Ponomarenko, L. A.; Morozov, S. V.; Gleeson, H. F.; Hill, E. W.; Geim, A. K.; Novoselov, K. S. Graphene-based liquid crystal device. *Nano Lett.* **2008**, *8*(6), 1704-1708.

[27] Mohanty, N.; Berry, V. Graphene-based single-bacterium resolution biodevice and dna transistor: interfacing graphene derivatives with nanoscale and microscale biocomponents. *Nano Lett.* **2008**, *8*(12), 4469-4476.

[28] Li, X.; Wang, X.; Zhang, L.; Lee, S.; Dai, H. Chemically derived, ultrasmooth graphene nanoribbon semiconductors. *Science* **2008**, *319*(5867), 1229-1232.

[29] Stankovich, D. S.; Dikin, D. A.; Dommett, G. H. B.; Kohlhaas, K. M.; Zimney, E. J.; Stach, E. A.; Piner, R. D.; Nguyen, S. T.; Ruoff, R. S. Graphene-based composite materials. *Nature* **2006**, *442*, 282-286.

[30] Xu, C.; Wang, X.; Zhu, J. Graphene - Metal particle nanocomposites. *J. Phys. Chem. C* **2008**, *112* (50), 19841-19845.

[31] Xu, Y.; Bai, H.; Lu, G.; Li, C.; Shi, G. Flexible graphene films via the filtration of water-soluble noncovalent functionalized graphene sheets. *J. Am. Chem. Soc.* **2008**, *130* (18), 5856-5857.

[32] Stankovich, S.; Dikin, D. A.; Piner, R. D.; Kohlhaas, K. A.; Kleinhammes, A.; Jia, Y.; Wu, Y.; Nguyen, S. T.; Ruoff, R. S. Synthesis of graphene-based nanosheets via chemical reduction of exfoliated graphite oxide. *Carbon* **2007**, *45*(7), 1558-1565.

[33] Hernandez, Y.; Nicolosi, V.; Lotya, M.; Blighe, F. M.; Sun, Z. Y.; De, S.; McGovern, I. T.; Holland, B.; Byrne, M.; Gun'ko, Y. K.; Boland, J. J.; Niraj, P.; Duesberg, G.; Krishnamurthy, S.; Goodhue, R.; Hutchison, J.; Scardaci, V.; Ferrari, A. C.; Coleman, J. N. High-yield production of graphene by liquid-phase exfoliation of graphite. *Nat. Nanotechnol.* **2008**, *3* (9), 563-568.

[34] Andersson, O. E.; Prasad, B. L. V.; Sato, H.; Enoki, T.; Hishiyama, Y.; Kaburagi, Y.; Yoshikawa, M.; Bandow, S. Structure and electronic properties of graphite nanoparticles. *Phys. Rev. B* **1998**, *58*, 16387-16395.

[35] Park, S.; Ruoff, R. S. Chemical methods for the production of graphenes. *Nat. Nanotechnol.* **2009**, *4*, 217-224.

[36] Li, D.; Kaner, R. B. Graphene-based materials. *Science* **2008**, *320*, 1170-1171.

[37] Stankovich, S.; Piner, R. D.; Chen, X.; Wu, N.; Nguyen, S. T.; Ruoff, R. S. Stable aqueous dispersions of graphitic nanoplatelets via the reduction of ex-

foliated graphite oxide in the presence of poly(sodium 4-styrenesulfonate). *J. Mat. Chem.* **2006**, *16*, 155-158.

[38] Niyogi, S.; Bekyarova, E.; Itkis, M. E.; McWilliams, J. L.; Hamon, M. A.; Haddon, R. C. Solution properties of graphite and graphene. *J. Am. Chem. Soc.* **2006**, *128*(24), 7720–7721.

[39] Dresselhaus, M. S.; Dresselhaus, G. Intercalation compounds of graphite. *Adv. Phys.* **2002**, *51*(1), 1-186.

[40] Celzard, A.; Mareche, J. F.; Furdin, G. Modelling of exfoliated graphite. *Prog. Mater. Sci.* **2005**, *50* (1), 93-179.

[41] Shioyama, H. The interactions of two chemical species in the interlayer spacing of graphite. *Syn. Met.* **2000**, *114* (1), 1-15.

[42] Doll, G. L.; Dresselhaus, G.; Dresselhaus, M. S.; Eklund, P. C.; Endo, M.; Holzwarth, N. A. W.; Issi, J. P.; Nicholls, J. T.; Schloegl, R.; Solin, S. A.; Tanuma, S.; Zabel, H. *Graphite intercalation compounds*, Springer: USA, **1992**; *Vol. 2.*

[43] Hwang, D. M.; Kirczenow, G.; Lagrange, P.; Magerl, A.; Moret, R.; Moss, S. C.; Setton, R.; Solin, S. A.; Zabel, H. *Graphite intercalation compounds*. Springer: USA, **1990**; *Vol. 1*.

[44] Tasis, D.; Tagmatarchis, N.; Bianco, A.; Prato, M. Chemistry of carbon nanotubes. *Chem. Rev.* **2006**, *106*(3), 1105-1136.

[45] Špitalský, Z.; Tasis, D.; Papagelis, K.; Galiotis, C. Carbon nanotube–polymer composites: Chemistry, processing, mechanical and electrical properties. *Prog. Polym. Sci.* **2010**, *35*, 357-401.

[46] Barrière, F.; Downard, A. J. Covalent modification of graphitic carbon substrates by non-electrochemical methods. *J. Solid State Electrochem.* **2008**, *12*, 1231-1244.

[47] Špitalský, Z.; Tsoukleri, G.; Tasis, D.; Krontiras, C.; Georga, S. N.; Galiotis, C. High volume fraction carbon nanotube–epoxy composites. *Nanotechnol.* **2009**, *20*, 405702 (405707pp).

[48] Špitalský, Z.; Aggelopoulos, C.; Tsoukleri, G.; Tsakiroglou, C.; Parthenios, J.; Georga, S.; Krontiras, C.; Tasis, D.; Papagelis, K.; Galiotis, C. The effect of oxidation treatment on the properties of multi-walled carbon nanotube thin films. *Mater. Sci. Eng. B* **2009**, *165*, 135-138.

[49] Dikin, D. A.; Stankovich, S.; Zimney, E. J.; Piner, R. D.; Dommett, G. H. B.; Evmenenko, G.; Nguyen, S. T.; Ruoff, R. S. Preparation and characterization of graphene oxide paper. *Nature* **2007**, *448*, 457-460.

[50] Park, S.; Lee, K.-S.; Bozoklu, G.; Cai, W.; Nguyen, S. T.; Ruoff, R. S. Graphene oxide papers modified by divalent ions – enhancing mechanical properties via chemical cross-linking. *ACS Nano* **2008**, *2*(3), 572-578.

[51] Brodie, B. C. On the atomic weight of graphite. *Philos. Trans.* **1859**, *149*, 249-259.

[52] Staudenmaier, L., Verfahren zur darstellung der graphitsäure. *Ber Leyns.* **1898**, *31*(2), 1481-1487.

[53] Hummers, W. S.; Offeman, R. E. Preparation of graphitic oxide. *J. Am. Chem. Soc.* **1958**, *80*(6), 1339-1339.

[54] Kontyukhova, N. I.; Ollivier, P. J.; Martin, B. R.; Mallouk, T. E.; Chizhik, S. A.; Buzaneva, E. V.; Gorchinskiy, A. D. Layer-by-Layer assembly of ultrathin composite films from micron-sized graphite oxide sheets and polycations. *Chem. Mater.* **1999**, *11*, 771-778.

[55] Luo, Z.; Lu, Y.; Somers, L. A.; Johnson, A. T. C. High yield preparation of macroscopic graphene oxide membranes. *J. Am. Chem. Soc.* **2009**, *131*, 898-899.

[56] Lerf, A.; He, H.; Riedl, T.; Forster, M.; Klinowski, J. ^{13}C and ^{1}H MAS NMR studies of graphite oxide and its chemically modified derivatives. *Solid State Ionics* **1997**, *101-103*, 857-862.

[57] Hamwi, A.; Marchand, V. Some chemical and electrochemical properties of graphite oxide. *J. Phys. Chem. Solids* **1996**, *57*(6-8), 867-872.

[58] Li, D.; Müller, M. B.; Gilje, S.; Kaner, R. B.; Wallace, G. G. Processable aqueous dispersions of graphene nanosheets. *Nat. Nanotechnol.* **2008**, *3*, 101-105.

[59] Rodríguez, A. M.; Jiménez, P. S. V. Some New Aspects of Graphite Oxidation at 0°C in a Liquid Medium. A mechanism proposal for oxidation to graphite oxide. *Carbon* **1986**, *24*(2), 163-167.

[60] Szabó, T.; Tombáca, E.; Illés, E.; Dékány, I. Enhanced acidity and pH-dependent surface charge characterization of successively oxidized graphite oxides. *Carbon* **2006**, *44*, 537-545.

[61] Hirata, M.; Gotou, T.; Horiuchi, S.; Fujiwara, M.; Ohba, M. Thin-film particles of graphite oxide 1: High-yield synthesis and flexibility of the particles. *Carbon* **2004**, *42*, 2929-2937.

[62] Rodríguez, A. M.; Jiménez, P. V. Thermal decomposition of the graphite oxidation products. *Thermochim. Acta* **1984**, *78*, 113-122.

[63] McAllister, M. J.; Li, J.-L.; Adamson, D. H.; Schniepp, H. C.; Abdala, A. A.; Liu, J.; Herrera-Alonso, M.; Milius, D. L.; Car, R.; Prud`homme, R. K.; Aksay, I. A. Single sheet functionalized graphene by oxidation and thermal expansion of graphite. *Chem. Mater.* **2007**, *19*, 4396-4404.

[64] Lerf, A.; He, H.; Forster, M.; Klinowski, J. Structure of graphite oxide revisited. *J. Phys. Chem. B* **1998**, *102*, 4477-4482.

[65] Cai, W.; Piner, R. D.; Stadermann, F. J.; Park, S.; Shaibat, M. A.; Ishii, Y.; Yang, D.; Velamakanni, A.; An, S. J.; Stoller, M.; An, J.; Chen, D.; Ruoff, R. S. Synthesis and solid-state nmr structural characterization of ^{13}C-Labeled graphite oxide. *Science* **2008**, *321*, 1815-1817.

[66] Nakajima, T.; Mabuchi, A.; Hagiwara, R. A new structure model of graphite oxide. *Carbon* **1988**, *26*(3), 357-361.

[67] Beckett, R. J.; Croft, R. C. The structure of graphite oxide. *J. Phys. Chem.* **1952**, *56*, 929-935.

[68] Cassagneau, T.; Guérin, F.; Fendler, J. H. Preparation and characterization of ultrathin films layer-by-layer self-assembled from graphite oxide nanoplatelets and polymers. *Langmuir* **2000**, *16*, 7318-7324.

[69] Cassagneau, T.; Fendler, J. H. High density rechargeable lithium-ion batteries self-assembled from graphite oxide nanoplatelets and polyelectrolytes. *Adv. Mater.* **1998**, *10*, 877-881.

[70] Fiang, J.; Beck, F. Thermodynamic data for anodic solid state graphite oxidation products in 96% sulphuric acid. *Carbon* **1992**, *30*(2), 223-228.

[71] Weng, W.-G.; Chen, G.-H.; Wu, D.-J.; Lin, Z.-Y.; Yan, W.-L. Preparation and characterizations of nanoparticles from graphite via an electrochemically oxidizing method. *Syn. Meter.* **2003**, *139*, 221-225.

[72] Matsuo, Y.; Sugie, Y. Preparation, structure and electrochemical property of pyrolytic carbon from graphite oxide. *Carbon* **1998**, *36*, 301-303.

[73] Schniepp, H. C.; Li, J. L.; McAllister, M. J.; Sai, H.; Herrera-Alonso, M.; Adamson, D. H.; Prud'homme, R. K.; Car, R.; Saville, D. A.; Aksay, I. A. Functionalized single graphene sheets derived from splitting graphite oxide. *J. Phys. Chem. B* **2006**, *110* (17), 8535-8539.

[74] Akhavan, O. The effect of heat treatment on formation of graphene thin films from graphene oxide nanosheets. *Carbon* **2010**, *48*(2), 509-519.

[75] Gómez-Navarro, C.; Weitz, R. T.; Bittner, A. M.; Scolari, M.; Mews, A.; Burghard, M.; Kern, K. Electronic transport properties of individual chemically reduced graphene oxide sheets. *Nano Lett.* **2007**, *7*(11), 3499-3503.

[76] Wei, Z.; Barlow, D. E.; Sheehan, P. E. The Assembly of single-layer graphene oxide and graphene using molecular templates. *Nano Lett.* **2008**, *8*(10), 3141-3145.

[77] Becerril, H. A.; Mao, J.; Liu, Z.; Stoltenberg, R. M.; Bao, Z.; Chen, Y. Evaluation of solution-processed reduced graphene oxide films as transparent conductors. *ACS Nano* **2008**, *2*(3), 463-470.

[78] Eda, G.; Fanchini, G.; Chhowalla, M. Large-area ultrathin films of reduced graphene oxide as a transparent and flexible electronic material. *Nat. Nanotechnol.* **2008**, *3*, 270-274.

[79] Kang, H.; Kulkarni, A.; Stankovich, S.; Ruoff, R. S.; Baik, S. Restoring electrical conductivity of dielectrophoretically assembled graphite oxide sheets by thermal and chemical reduction techniques. *Carbon* **2009**, *47*, 1520-1525.

[80] Kotov, N. A.; Dékány, I.; Fendler, J. H. Ultrathin Graphite oxide-polyelectrolyte composites prepared by self-assembly: Transition between conductive and non-conductive states. *Adv. Mater.* **1996**, *8* (8), 637-641.

[81] Liu, P.; Gong, K. Synthesis of polyaniline-intercalated graphite oxide by an in situ oxidative polymerization reaction. *Carbon* **1999**, *37*, 706-707.

[82] Bourlinos, A. B.; Gournis, D.; Petridikis, D.; Szabó, T.; Szeri, A.; Dékány, I. Graphite Oxide: Chemical Reduction to Graphite and Surface Modification with Primary Aliphatic Amines and Amino Acids. *Lamgmuir* **2003**, *19*, 6050-6055.

[83] Fan, X.; Peng, W.; Li, Y.; Li, X.; Wang, S.; Zhang, G.; Zhang, F. Deoxygenation of exfoliated graphite oxide under alkaline condition: A green route to graphene preparation. *Adv. Mater.* **2008**, *20*, 4490-4493.

[84] Chen, W.; Yan, L.; Bangal, P. R. Preparation of graphene by the rapid and mild thermal reduction of graphene oxide induced by microwaves. *Carbon* **2010**, *48(4)*, 1146-1152.

[85] Du, X. S.; Xiao, M.; Meng, Y. Z.; Hay, A. S. Direct synthesis of poly(arylenedisulfide)/carbon nanosheet composites via the oxidation with graphite oxide. *Carbon* **2005**, *43*, 195-213.

[86] Li, F.; Song, J.; Yang, H.; Gan, S.; Zhang, Q.; Han, D.; Ivaska, A.; Niu, L. One-step synthesis of graphene/SnO_2 nanocomposites and its application in electrochemical supercapacitors. *Nanotechnol.* **2009**, *20*, 455602(455606pp).

[87] Kim, S. R.; Parvez, M. K.; Chhowalla, M. UV-reduction of graphene oxide and its application as an interfacial layer to reduce the back-transport reactions in dye-sensitized solar cells. *Chem. Phys. Lett.* **2009**, *483*(1-3), 124-127.

[88] Cote, L. J.; Cruz-Silva, R.; Huang, J. Flash reduction and patterning of graphite oxide and its polymer composites. *J. Am. Chem. Soc.* **2009**, *131* (31), 11027-11032.

[89] Williams, G.; Seger, B.; Kamat, P. V. TiO_2-Graphene Nanocomposites. UV-assisted photocatalytic reduction of graphene oxide. *ACS Nano* **2008**, *2*(7), 1487-1491.

[90] Muszynski, R.; Seger, B.; Kamat, P. V. Decorating graphene sheets with gold nanoparticles. *J. Phys. Chem. C* **2008**, *112*(14), 5263-5266.

[91] Liu, Z.-B.; Xu, Y.-F.; Zhang, X.-Y.; Zhang, X.-L.; Chen, Y.-S.; Tian, J.-G. Porphyrin and fullerene covalently functionalized graphene hybrid materials with large nonlinear optical properties. *J. Phys. Chem. B* **2009**, *113*, 9681-9686.

[92] Xu, Y.; Liu, Z.; Zhang, X.; Wang, Y.; Tian, J.; Huang, Y.; Ma, Y.; Zhang, X.; Chen, Y. A graphene hybrid material covalently functionalized with porphyrin: synthesis and optical limiting property. *Adv. Mater.* **2009**, *21*, 1275-1279.

[93] Karousis, N.; Economopoulos, S. P.; Sarantopoulou, E.; Tagmatarchis, N. Porphyrin counter anion in imidazolium-modified graphene-oxide. *Carbon* **2010**, *48*(3), 854-860.

[94] Liu, Z.; Robinson, J. T.; Sun, X.; Dai, H. PEGylated Nanographene oxide for delivery of water-insoluble cancer drugs. *J. Am. Chem. Soc.* **2008**, *130*, 10876-10877.

[95] Salavagione, H. J.; Gómez, M. A.; Martínez, G. Polymeric Modification of graphene through esterification of graphite oxide and poly(vinyl alcohol). *Macromol.* **2009**, *42*(17), 6331-6334.

[96] Veca, L. M.; Lu, F.; Meziani, M. J.; Cao, L.; Zhang, P.; Qi, G.; Qu, L.; Shrestha, M.; Sun, Y.-P. Polymer functionalization and solubilization of carbon nanosheets. *Chem. Commun.* **2009**, 2565-2567.

[97] Stankovich, S.; Piner, R. D.; Nguyen, S. T.; Ruoff, R. S. Synthesis and exfoliation of isocyanate-treated graphene oxide nanoplatelets. *Carbon* **2006**, *44*, 3342–3347.

[98] Wang, G.; Wang, B.; Park, J.; Yang, J.; Shen, X.; Yao, J. Synthesis of enhanced hydrophilic and hydrophobic graphene oxide nanosheets by a solvothermal method. *Carbon* **2009**, *47*(1), 68-72

[99] Lee, S. H.; Dreyer, D. R.; An, J.; Velamakanni, A.; Piner, R. D.; Park, S.; Zhu, Y.; Kim, S. O.; Bielawski, C. W.; Ruoff, R. S. Polymer brushes via controlled, surface-initiated atom transfer radical polymerization (ATRP) from graphene oxide. *Macromol. Rapid Commun.* **2010**, *31*(3), 281-288.

[100] Yang, Y.; Wang, J.; Zhang, J.; Liu, J.; Yang, X.; Zhao, H. Exfoliated graphite oxide decorated by PDMAEMA chains and polymer particles. *Lamgmuir* **2009**, *25*(19), 11808-11814.

[101] Matsuo, Y.; Fukunaga, T.; Fukutsuka, T.; Sugie, Y. Silylation of graphite oxide. *Carbon* **2004**, *42*, 2117-2119.

[102] Matsuo, Y.; Tabata, T.; Fukunaga, T.; Fukutsuka, T.; Sugie, Y. Preparation and characterization of silylated graphite oxide. *Carbon* **2005**, *43*, 2875-2882.

[103] Subrahmanyam, K. S.; Ghosh, A.; Gomathi, A.; Govindaraj, A.; Rao, C. N. R. Covalent and noncovalent functionalization and solubilization of graphene. *Nanosci. Nanotechnol. Lett.* **2009**, *1*, 28-31.

[104] Herrera-Alonso, M.; Abdala, A. A.; McAllister, M. J.; Aksay, I. A.; Prud'homme, R. K. Intercalation and Stitching of Graphite Oxide with Diaminoalkanes. *Lamgmuir* **2007**, *23*, 10644-10649.

[105] Shan, C.; Yang, H.; Han, D.; Zhang, Q.; Ivaska, A.; Niu, A. Electrochemical determination of NADH and ethanol based on ionic liquid-functionalized graphene. *Biosens. Bioelectr.* **2010**, *25(6)*, 1504-1508.

[106] Yang, H.; Shan, C.; Li, F.; Han, D.; Zhang, Q.; Niu, L. Covalent functionalization of polydisperse chemically-converted graphene sheets with amine-terminated ionic liquid. *Chem. Commun.* **2009**, 3880-3882.

[107] Wang, S.; Chia, P.-J.; Chua, L.-L.; Zhao, L.-H.; Png, R.-Q.; Sivaramakrishnan, S.; Zhou, M.; Goh, R. G.-S.; Friend, R. H.; Wee, A. T.-S.; Ho, P. K.-H. Band-like transport in surface-functionalized highly solution-processable graphene nanosheets. *Adv. Mater.* **2008**, *20*, 3440-3446.

[108] Wang, G.; Shena, X.; Wang, B.; Yao, J.; Park, J. Synthesis and characterization of hydrophilic and organophilic graphene nanosheets. *Carbon* **2009**, *47*, 1359-1364.

[109] Chattopadhyay, J.; Mukherjee, A.; Chakraborty, S.; Kang, J.; Loos, P. J.; Kelly, K. F.; Schmidt, H. K.; Billups, W. E. Exfoliated soluble graphite. *Carbon* **2009**, *47*(13), 2945-2949.

[110] Chakraborty, S.; Chattopadhyay, J.; Guo, W.; Billups, W. E. Functionalization of potassium graphite. *Angew. Chem. Int. Ed.* **2007**, *46*(24), 4486-4488.

[111] Bon, S. B.; Valentini, L.; Verdejo, R.; Fierro, J. L. G.; Peponi, L.; Lopez-Manchado, M. A.; Kenny, J. M. Plasma fluorination of chemically derived graphene sheets and subsequent modification with butylamine. *Chem. Mat.* **2009**, *21*, 3433-3438.

[112] Chakraborty, S.; Guo, W.; Hauge, R. H.; Billups, W. E. Reductive Alkylation of Fluorinated Graphite. *Chem. Mat.* **2008**, *20* (9), 3134-3136.

[113] Worsley, K. A.; Ramesh, P.; Mandal, S. K.; Niyogi, S.; Itkis, M. E.; Haddon, R. C. Soluble graphene derived from graphite fluoride. *Chem. Phys. Lett.* **2007**, *445* (1-3), 51-56.

[114] Bekyarova, E.; Itkis, M. E.; Ramesh, P.; Berger, C.; Sprinkle, M.; de Heer, W. A.; Haddon, R. C. Chemical modification of epitaxial graphene: spontaneous grafting of aryl groups. *J. Am. Chem. Soc.* **2009**, *131* (4), 1336-1337.

[115] Lomeda, J. R.; Doyle, C. D.; Kosynkin, D. V.; Hwang, W.-F.; Tour, J. M. Diazonium functionalization of surfactant-wrapped chemically converted graphene sheets. *J. Am. Chem. Soc.* **2008**, *130*(48), 16201-16206.

[116] Si, Y.; Samulski, E. T. Synthesis of water soluble graphene. *Nano Lett.* **2008**, *8*(6), 1679-1682.

[117] Xu, Y.; Wang, Y.; Liang, J.; Huang, Y.; Ma, Y.; Wan, X.; Chen, Y. A hybrid material of graphene and poly (3,4-ethyldioxythiophene) with high conductivity, flexibility, and transparency. *Nano Res.* **2009**, *2*, 343-348.

[118] Fang, M.; Wang, K.; Lu, H.; Yang, Y.; Nutt, S. Covalent polymer functionalization of graphene nanosheets and mechanical properties of composites. *J. Mater. Chem.* **2009**, *19*, 7098-7105.

[119] Choi, J.; Kim, K.-j.; Kim, B.; Lee, H.; Kim, S. Covalent functionalization of epitaxial graphene by azidotrimethylsilane. *J. Phys. Chem. C* **2009**, *113*(22), 9433-9435.

[120] Hamilton, C. E.; Lomeda, J. R.; Sun, Z.; Tour, J. M.; Barron, A. R. High-yield organic dispersions of unfunctionalized graphene. *Nano Lett.* **2009**, *9*(10), 3460-3462.

[121] Liu, N.; Luo, F.; Wu, H.; Liu, Y.; Zhang, C.; Chen, J. One-step ionic-liquid-assisted electrochemical synthesis of ionic-liquid-functionalized graphene sheets directly from graphite. *Adv. Funct. Mater.* **2008**, *18*, 1518-1525.

[122] Shen, J.; Hu, Y.; Li, C.; Qin, C.; Shi, M.; Ye, M. Layer-by-Layer Self-Assembly of Graphene Nanoplatelets. *Lamgmuir* **2009**, *25*(11), 6122-6128.

[123] Shen, J.; Hu, Y.; Li, C.; Qin, C.; Ye, M. Synthesis of amphiphilic graphene nanoplatelets. *Small* **2009**, *5*(1), 82-85.

[124] Hu, H.; Wang, X.; Wang, J.; Wan, L.; Liu, F.; Zheng, H.; Chen, R.; Xu, C. Preparation and properties of graphene nanosheets–polystyrene nanocomposites via in situ emulsion polymerization. *Chem. Phys. Lett.* **2010**, *484(*4-6*)*, 247-253.

[125] Liu, H.; Ryu, S.; Chen, Z.; Steigerwald, M. L.; Nuckolls, C.; Brus, L. E. Photochemical reactivity of graphene. *J. Am. Chem. Soc.* **2009**, *131*(47), 17099-17101.

[126] Ryu, S.; Han, M. Y.; Maultzsch, J.; Heinz, T. F.; Kim, P.; Steigerwald, M. L.; Brus, L. E. Reversible basal plane hydrogenation of graphene. *Nano Lett.* **2008**, *8*(12), 4597-4602.

[127] Elias, D. C.; Nair, R. R.; Mohiuddin, T. M. G.; Morozov, S. V.; Blake, P.; Halsall, M. P.; Ferrari, A. C.; Boukhvalov, D. W.; Katsnelson, M. I.; Geim, A. K.; Novoselov, K. S. Control of graphene's properties by reversible hydrogenation: Evidence for graphane. *Science* **2009**, *323*(5914), 610-613.

Received: 31 December, 2009 Revised: 04 March, 2010 Accepted: 16 March, 2010